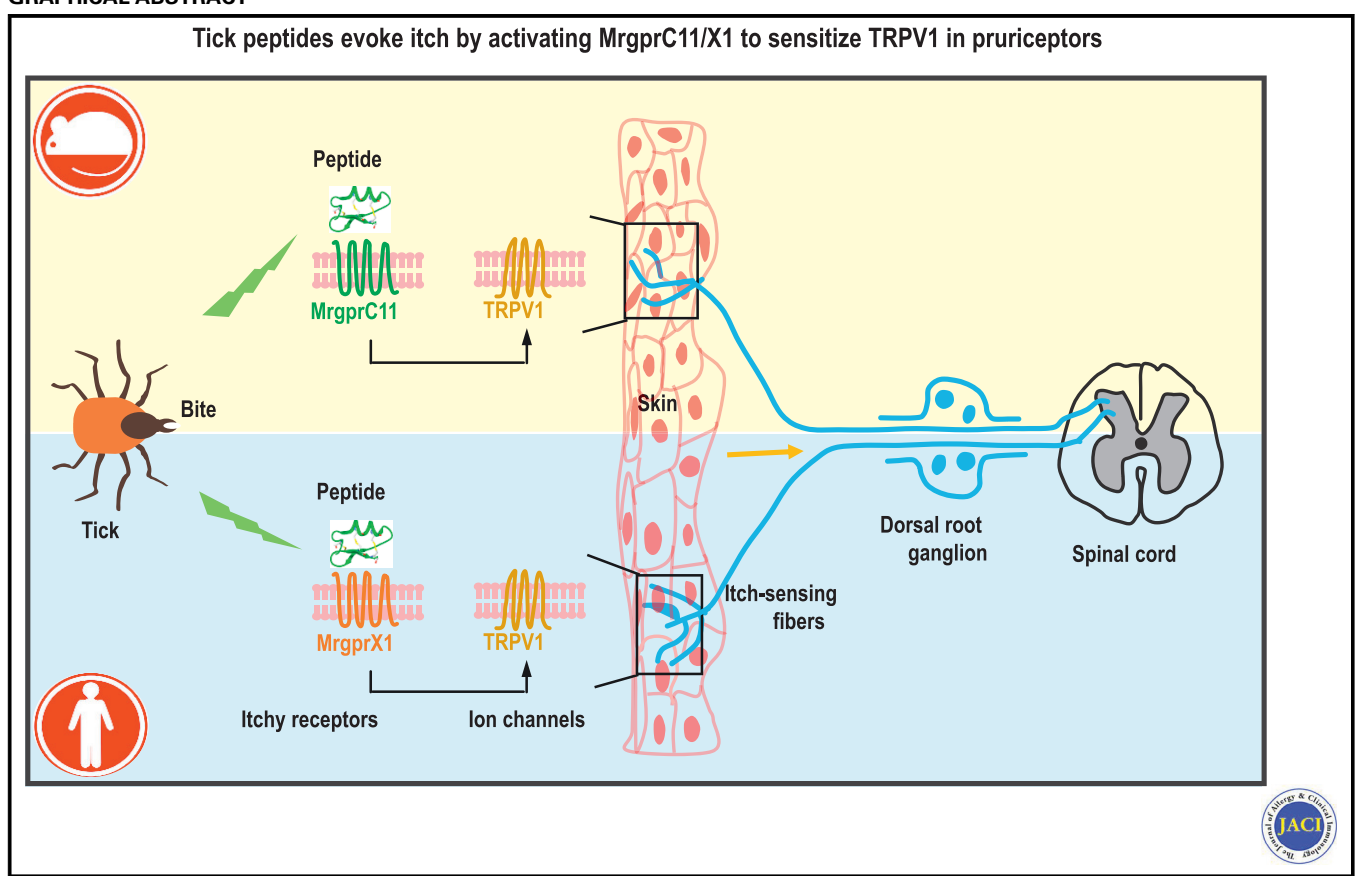
# Tick peptides evoke itch by activating MrgprC11/MRGPRX1 to sensitize TRPV1 in pruriceptors



Xueke Li, MSc, a\* Haifeng Yang, MSc, a\* Yuewen Han, MSc, Shijin Yin, PhD, Bingzheng Shen, PhD, Yingliang Wu, PhD, Wenxin Li, PhD, and Zhijian Cao, PhD, Wuhan, China

#### **GRAPHICAL ABSTRACT**



Background: Tick bites severely threaten human health because they allow the transmission of many deadly pathogens, including viruses, bacteria, protozoa, and helminths. Pruritus is a leading symptom of tick bites, but its molecular and neural bases remain elusive.

Objectives: This study sought to discover potent drugs and targets for the specific prevention and treatment of tick bite-induced pruritus and arthropod-related itch.

From <sup>a</sup>the State Key Laboratory of Virology, College of Life Sciences; <sup>c</sup>the Bio-drug Research Center; and <sup>d</sup>the Hubei Province Engineering and Technology Research, Center for Fluorinated Pharmaceuticals, Wuhan University; and <sup>b</sup>the School of Pharmaceutical Sciences, South-Central University for Nationalities, Wuhan.

\*These authors contributed equally to this work.

Supported by grants from National Science Fund of China (32070525, 31872239, and 81630091), Hubei Science Fund for Excellent Scholars (2020CFA015), and the Open Research Program of the State Key Laboratory of Virology of China (2020KF002).

Disclosure of potential conflict of interest: The authors declare that they have no relevant conflicts of interest.

Methods: We used live-cell calcium imaging, patch-clamp recordings, and genetic ablation and evaluated mouse behavior to investigate the molecular and neural bases of tick bite-induced pruritus.

Results: We found that 2 tick salivary peptides, IP defensin 1 (IPDef1) and IR defensin 2 (IRDef2), induced itch in mice. IPDef1 was further revealed to have a stronger pruritogenic potential than IRDef2 and to induce pruritus in a

Received for publication May 4, 2020; revised November 21, 2020; accepted for publication December 2, 2020.

Available online December 22, 2020.

Corresponding author: Zhijian Cao, PhD, State Key Laboratory of Virology, College of Life Sciences, Wuhan University, Wuhan 430072, China. E-mail: zjcao@whu.edu.cn.

The CrossMark symbol notifies online readers when updates have been made to the article such as errata or minor corrections 0091-6749

© 2020 The Authors. Published by Elsevier Inc. on behalf of the American Academy of Allergy, Asthma & Immunology. This is an open access article under the CC BY-NC-ND license (http://creativecommons.org/licenses/by-nc-nd/4.0/). https://doi.org/10.1016/j.jaci.2020.12.626

histamine-independent manner. IPDef1 evoked itch by activating mouse MrgprC11 and human MRGPRX1 on dorsal root ganglion neurons. IPDef1-activated MrgprC11/X1 signaling sensitized downstream ion channel TRPV1 on dorsal root ganglion neurons. Moreover, IPDef1 also activated mouse MrgprB2 and its ortholog human MRGPRX2 selectively expressed on mast cells, inducing the release of inflammatory cytokines and driving acute inflammation in mice, although mast cell activation did not contribute to oxidated IPDef1-induced itch.

Conclusions: Our study identifies tick salivary peptides as a new class of pruritogens that initiate itch through MrgprC11/X1-TRPV1 signaling in pruritoceptors. Our work will provide potential drug targets for the prevention and treatment of pruritus induced by the bites or stings of tick and maybe other arthropods. (J Allergy Clin Immunol 2021;147:2236-48.)

Key words: Tick, peptide, itch, Mrgprs, TRP channel

Pruritus is a dermatological symptom involving skin itching but no primary skin damage and is the most common clinical manifestation of skin diseases. <sup>1,2</sup> There are numerous factors that can induce pruritus, such as cold, warmth, chemical fibers, bites of ticks and insects, diabetes, liver disease, and kidney disease. In addition to the H1/H4 receptor, Mrgprs and Piezo2 channels were recently identified as itch-related membrane proteins. <sup>3,4</sup> However, itch is still an unmet clinical problem with no universal treatment because the molecular, cellular, and neural circuit mechanisms of itch have not been fully understood. Therefore, it is important to identify new and specific pruritogens to dissect molecular and cellular mechanisms of itch as well as unravel the specificity and selectivity of itch receptors.

The bites or stings of many arthropods are among the most common causes of itching.<sup>5,6</sup> These arthropods mainly include insects and arachnids, such as fleas, mosquitoes, bedbugs, bees, wasps, mites, and ticks. Each of them has thousands of species on the earth, constituting a large group of itch-related organisms. Ticks are small arachnids that belong to the order Ixodida of the class Arachnida. There are approximately 900 tick species in the world. Blood-sucking ticks attack various types of vertebrates. Moreover, some tick species carry pathogens such as viruses and rickettsiae, which can infect humans and animals. 7,8 Tick bites can lead to local lesions and systemic illness, referred to as tick toxicosis. Pruritus is a leading symptom of tick toxicosis. Patients bitten by lone star ticks exhibit skin manifestations, specifically a large number of pruritic papules. Dogs bitten by the mouro tick Ornithodoros brasiliensis also present skin rash and itch symptoms. 10 However, the molecular and neural bases of tick bite-induced pruritus is largely unknown.

The saliva or venoms of the itch-inducing arthropods contain various toxic peptides used for prey and defense that exhibit extremely diverse primary sequences, spatial structures, targeting receptors, and biological functions. <sup>11-15</sup> It is possible that these arthropods may produce a class of common peptides that induce itch in humans and animals. Previous reports showed that the class of the ancient invertebrate defensin could serve as a common peptide component in the saliva or venoms of the itch-inducing arthropods. <sup>16,17</sup> We speculated that these ancient invertebrate defensin peptides may be potent candidate pruritogens.

Abbreviations used

AITC: Allyl isothiocyanate BAM: Bovine adrenal medulla

Cap: Capsaicin

CETY: H1R antagonist cetirizine

CQ: Chloroquine

CRISPR: Clustered regularly interspaced short palindromic repeats

DRG: Dorsal root ganglion

EC<sub>50</sub>: Concentration for 50% of maximal effect

HEK293T: Human embryonic kidney 293T

HIS: Histamine His: Histidine IPDef1: IP defensin 1

IP-O: Oxidated form of IPDef1IP-R: Reduced form of IPDef1

IRDef2: IR defensin 2

JNJ: H4R antagonist JNJ7777120

MALDI: Matrix-assisted laser desorption ionization

MCP-1: Monocyte chemotactic protein 1 MIC: Minimum inhibitory concentration PAMP: Pro-adrenomedullin peptide

PMC: Peritoneal mast cell qRT-PCR: Quantitative RT-PCR

WT: Wild-type

In this study, 2 tick salivary defensin peptides, IP defensin 1 (IPDef1) and IR defensin 2 (IRDef2), were found to induce histamine (HIS)-independent itch in mice while IPDef1 had a stronger activity. IPDef1 produced itch through directly activating dorsal root ganglion (DRG) neurons and triggering Ca<sup>2+</sup> influx. Using live cell calcium imaging, patch-clamp recordings, coimmunoprecipitation, and gene editing, mouse MrgprC11 and human MRGPRX1 were identified as the main itchy receptors for IPDef1 on DRG neurons. The MrgprC11/X1-TRPV1 axis in DRG neurons was an important signaling pathway for IPDef1induced itch. Interestingly, IPDef1 also activated mouse MrgprB2 and its human ortholog MRGPRX2 selectively expressed on mast cells, thereby causing inflammatory cytokine release and inducing acute inflammation in mice. Unexpectedly, mast cell activation by IPDef1 did not contribute to its itch-inducing activity. Our study discloses the molecular and cellular basis of itch induced by the tick salivary peptides and provides potential drug targets for the prevention and treatment of pruritus induced by the bites or stings of arthropods such as ticks, mosquitoes and ants.

#### **METHODS**

#### Oxidative refolding and homology modeling

Reduced IPDef1 and IRDef2 were synthesized by ChinaPeptides Co, Ltd (Shanghai, China), and the purity of each peptide was >97%. To form 3 disulfide linkages via intermolecular oxidative refolding, the reduced peptides (1 mg) were dissolved in 2 mL Tris-HCl buffer (0.1 mol/L, pH 8.0) and incubated at 25°C for 48 hours with continuous shaking at 50 rev/min. The oxidized peptides were centrifuged at 12,000 rev/min for 10 minutes at 4°C, and the supernatants were purified by RP-HPLC (Agilent Technologies, Santa Clara, Calif). The average molecular mass of each oxidized peptide was confirmed by matrix-assisted laser desorption ionization (MALDI) time-of-flight mass spectrometry (BiflexIII; Bruker Daltonik GmbH, Bremen, Germany). Oxidized IPDef1 (IP-O) and IRDef2, which were desalinated and purified by RP-HPLC, were mixed with MALDI-matrix solution (1 mL, containing 10 mg/mL  $\alpha$ -cyano-4-hydroxycinnamic acid, 0.1% trifluoroacetic

2238 LI ET AL

J ALLERGY CLIN IMMUNOL

JUNE 2021

acid, and 45% acetonitrile). Then, 1  $\mu L$  of each peptide sample mixture was spotted onto a MALDI target plate and left to air-dry at room temperature. Mass spectrometry was performed with FlexControl software (version 3.0; Bruker Daltonics, Billerica, Mass) for a mass range of mass-to-charge ratio from 1000 to 8000 Da. The mass of the oxidized peptide was measured in positive-ion linear mode at an accelerating voltage of 25 kV. The secondary structure of each peptide was determined by circular dichroism spectroscopy using a JASCO J-810 spectrometer (JASCO International Co, Ltd, Tokyo, Japan). The peptides were dissolved in Milli-Q water at a concentration of approximately 200 µg/mL. Circular dichroism spectra were obtained at wavelengths from 190 nm to 260 nm at room temperature (25°C). The scanning speed was 50 nm/min, the resolution was 1 nm, and the response time was 2 seconds. Each reading was repeated 3 times, and the results are shown as the mean residue molar ellipticity ( $\theta$ ). The 3-dimensional–structure prediction was determined using SWISS-MODEL Interactive Workspace (http:// swissmodel.expasy.org).

#### In vitro antimicrobial assays

Reference strains of gram-positive bacteria and gram-negative bacteria were used to evaluate the in vitro antimicrobial activity of IPDef1 (reduced [IP-R] and IP-O). Staphylococcus aureus AB94004, S aureus ATCC25923, S aureus ATCC6538, Micrococcus luteus AB93113, Bacillus subtilis AB91021, Escherichia coli AB94012, and E coli ATCC25922 were purchased from the China Center of Type Culture Collection (Wuhan, China). The antimicrobial activities of IP-R and IP-O in vitro were evaluated by a 2-fold serial dilution method as recommended by Clinical and Laboratory Standards Institute guidelines. The strains, which were stored in a refrigerator at  $-80^{\circ}$ C, were inoculated into solid medium plates and cultivated at 37 °C overnight in a thermostatic incubator. A single colony was selected and subcultured in liquid medium. After overnight culturing and activation, the test strains were diluted with medium to  $10^4$  to  $10^6$  colony forming units/mL. Then,  $20 \,\mu\text{L}$  peptide at various concentrations was added to  $80\,\mu L$  diluted culture medium containing the test strains for a total volume of  $100 \,\mu L$ . The 96-well microplates were incubated at 37 °C with continuous shaking at 100 rev/min for 14 to 16 hours, and the absorbance at 630 nm was measured to determine the minimum inhibitory concentration (MIC). The MIC was defined as the lowest peptide concentration that completely prevented growth and was measured with a microtiter optical plate reader. To monitor the validity and reproducibility of the assays, incubations were performed in triplicate with 3 parallel replicates.

#### **Behavioral studies**

Two- to 3-month-old male mice (C57BL/6, 20-30 g) were housed on a 12hour light-dark cycle at 24°C. On the day of the experiment, the animals were allowed to acclimatize to the test chamber for 10 minutes prior to injection. A pruritic substance (ie, IPDef1, IRDef2, HIS, chloroquine [CQ], proadrenomedullin peptide [PAMP]9-20, or anti-IgE) was intradermally injected into the nape of the neck after acclimatization. A bout of scratching was defined as an episode in which a mouse lifted its paw and scratched directly at the area around the injection site continuously for any length of time and lasted until the paw was returned to the floor. The use of both forepaws was classified as grooming behavior and was not considered scratching. Scratching behavior was quantified by counting the number of scratching bouts during the 30minute observation period. An antagonist (ie, cetirizine, JNJ7777120, AMG9810, or HC030031) or the mast cell stabilizer cromolyn sodium were intraperitoneally injected 30 minutes before the injection of the pruritic substances. All behavioral tests were performed by an experimenter blind to genotype. All experiments were performed under the policies and recommendations of the Institutional Animal Care and Use Committee of Wuhan University. Antagonists listed above were purchased from TargetMol (Target Molecule Corp, Boston, Mass).

#### Gene amplification

Because Mrgprs are expressed mainly in the peripheral and central nervous systems, we extracted total RNA from mouse DRG neurons using TRIzol

reagent (BBI, Toronto, Ontario, Canada). Then, total RNA was reverse-transcribed into the first-strand cDNA using the First Strand cDNA Synthesis Kit (Thermo Fisher Scientific, Waltham, Mass). Subsequently, the synthesized cDNAs were used as templates for random primer p(dN)6 amplification by PCR. The mouse *Mrgpr* and human *MRGPR* genes were amplified and characterized by PCR. Experiments involving tissue were also performed under the policies and recommendations of the Institutional Animal Care and Use Committee of Wuhan University.

#### **DRG** neuron culture

DRG neurons from all spinal levels were collected from 4- to 5-week-old mice, placed in cold HBSS, and treated with enzyme solution at 37°C. Briefly, neurons from sensory ganglia were dissected and incubated for 10 minutes in 1.4 mg/mL collagenase P (Roche, Basel, Switzerland) in Hanks calcium-free balanced salt solution. The neurons were then incubated in HBSS with 0.25% standard trypsin (vol/vol) for 3 minutes with gentle agitation. After trituration and centrifugation, the cells were resuspended in media (Eagle's modified Eagle medium with Earle's balance salt solution medium supplemented with 10% bovine serum [vol/vol], modified Eagle medium vitamins, penicillin/ streptomycin, and l-glutamine), plated on glass coverslips coated with poly-Dlysine, cultured in an incubator at 37°C and used within 18 hours. All results were also confirmed using neuronal cultures from adult mice.

#### **HEK293T cell culture**

Human embryonic kidney 293T (HEK293T) cells were cultured on poly-D-lysine-coated glass coverslips. The cells were transfected with 500 ng mouse *Mrgprs*, 500 ng human *MRGPRs*, 250 ng human *TRPA1*, or 250 ng human *TRPV1* plasmids with TurboFect (Invitrogen, Thermo Fisher Scientific). The cells were replated on glass coverslips 20 hours after transfection and used for calcium imaging or patch-clamp recordings.

#### Calcium imaging

DRG neurons or HEK293T cells were loaded for 30 to 45 minutes in the dark with 10 µmol/L Fura-2AM (Yeasen Biotech Co, Ltd, Shanghai, China) supplemented with 0.01% Pluronic F-127 (wt/vol; Yeasen Biotech Co, Ltd) in physiological Ringer's solution containing 140 mmol/L NaCl, 5 mmol/L KCl, 10 mmol/L HEPES, 2 mmol/L CaCl2, 2 mmol/L MgCl2 and 10 mmol/L d-(+)-glucose, pH 7.4. After washing, the cells were imaged at an excitation wavelength of 340 and 380 nm to detect intracellular free calcium. Cells were considered to have exhibited a response if the [Ca<sub>2</sub><sup>+</sup>]<sub>i</sub> rose by at least 30% for at least 10 seconds, allowing us to clearly distinguish ligandinduced responses from random flickering events. Each experiment was performed at least 3 times with at least 100 neurons or HEK293T cells were analyzed. For the assay of calcium response traces, each colored line represents an individual DRG neuron or HEK293T cell. For the assay of concentration for 50% of maximal effect (EC50) value or the response prevalence, calcium responses at each concentration or substance were normalized to the maximal response elicited subsequently. Each point represents data collected from an independent experiment. KCl (50 mmol/L) was used to identify live cells. Bovine adrenal medulla (BAM)8-22 (50 µmol/L), CQ (1 mmol/L), or PAMP9-20 (20 µmol/L) was used as an agonist to identify the functional MrgprC11/MRGPRX1, MrgprA3, or MrgprB2, respectively. Capsaicin (Cap; 1 μmol/L) or allyl isothiocyanate (AITC; 100 μmol/L) was used as a channel agonist to identify the functional TRPV1 or TRPA1, respectively. Calcium imaging assays were performed by an experimenter blind to genotype or pretreatment.

#### Whole-cell patch-clamp recordings

HEK293T cells plated on coverslips were transferred to a chamber with extracellular solution. Patch pipettes with a resistance of 2 to 4  $M\Omega$  were used. For current-clamp recordings, action potentials were measured with an Axon 700B amplifier and the pCLAMP 9.2 software package (Axon Instruments, Union City, Calif). Cells were perfused with IP-O (10  $\mu$ mol/L) for 30 seconds,

and Cap (1  $\mu$ mol/L) or AITC (100  $\mu$ mol/L) was used as a positive control. All experiments were performed at room temperature (25°C).

#### **Knockout mice**

The 3 knockout mouse strains we used were on the C57BL/6 background. MrgprC11 knockout mice were generated by the following strategy (Cyagen Biosciences, Santa Clara, Calif). The *MrgprC11* gene (NCBI Reference Sequence: NM\_207540; Ensembl: ENSMUSG00000070552) is located on mouse chromosome 7. Two exons with the ATG start codon in exon 2 and the TGA stop codon in exon 2 were identified (Transcript: ENSMUST00000094390). Exon 2 was selected as the target site. Clustered regularly interspaced short palindromic repeats (CRISPR)-associated protein 9, or Cas9, and guide RNA were coinjected into fertilized eggs to produce knockout mice. The pups were genotyped by PCR followed by sequencing analysis. Exon 2 starts from approximately 0.1% of the coding region. Exon 2 covers 100.0% of the coding region. The size of the effective knockout region was 964 bp. The knockout region did not contain any other known gene. *Trpa1*<sup>-/-</sup> and *Trpv1*<sup>-/-</sup> mice were obtained from Jackson Laboratory (Bar Harbor, Me).

#### **Immunoprecipitation**

Cells transfected with the plamid pcDNA3.1 expressing N-flag-tagged Mrgpr receptors (mouse MrgprA3/C11 and human MRGPRX1/X2/X3/X4) and TRP channels (TRPV1 and TRPA1) were washed with ice-cold PBS, and proteins were extracted according to the manufacturer's instructions. Control represents HEK293T cells transfected with the plamid pcDNA3.1-Flag. After centrifugation, an adequate amount of soluble His–IP-O was added to the supernatant, and the mixture was incubated with rotation for 4 hours at a temperature of 4°C. Subsequently, 8  $\mu$ L protein G beads and 0.5  $\mu$ L anti-Flag antibody (Sigma-Aldrich, St Louis, Mo) were added, and the samples were incubated with rotation overnight. After overnight incubation, the Sepharose beads were washed 3 times with ice-cold modified NHG buffer (150 mmol/L NaCl, 50 mmol/L HEPES, 10% glycerol, 1% Triton X-100, pH 7.2) and resuspended in 5× SDS sample buffer. The samples were separated by SDS-PAGE and then transferred onto Immobilon-P membranes (Millipore, Burlington, Mass) for Western blot analysis.

#### Peritoneal mast cell purification and imaging

Three- to 4-month-old adult C57BL/6 male and female mice were killed by CO2 inhalation. Ice-cold mast cell dissociation media (HBSS with 3% FBS and 10 mmol/L HEPES, pH 7.2) was used to perform 2 sequential peritoneal lavages; the media from these lavages were combined, and the cells were spun down at 200g. The pellet from each mouse was resuspended in 2 mL mast cell dissociation media, layered on top of 4 mL isotonic 70% Percoll suspension (2.8 mL Percoll, 320  $\mu L$  10× HBSS, 40  $\mu L$  1 mol/L HEPES, 830  $\mu L$  mast cell dissociation media), and spun down for 20 minutes with 500g at 4°C. Mast cells were recovered in the pellet. Purity was assayed by toluidine blue staining. Mast cells were resuspended at a concentration of  $5 \times 10^5$  to  $1 \times 10^6$  cells/mL in Dulbecco modified Eagle medium with 10% FBS and 25 ng/mL recombinant mouse stem cell factor (Sigma-Aldrich) and allowed to recover for 2 hours in a 37°C incubator with 5% CO2. The cells were then spun down, resuspended in HBSS, counted, and plated at a concentration of 300 cells/well in 75  $\mu L$  HBSS in 96-well plates. After 2 hours of incubation at 37°C and 5% CO<sub>2</sub>, the mast cells were used for calcium imaging according to the methods described above.

#### Hind paw swelling and Evans blue extravasation

Adult male C57BL/6 mice were anesthetized by intraperitoneal injection of 0.2 mL chloral hydrate (3.5%). Fifteen minutes after induction of anesthesia, the mice were injected with 50  $\mu L$  12.5 mg/mL Evans blue (Sigma-Aldrich) in saline through the tail vein. Five minutes after Evans blue injection, the test substance (IP-O, 2 mg/mL, 5  $\mu L)$  was intraplantarly injected into one hind paw of each mouse, and saline (5  $\mu L)$  was injected into the other hind paw. Paw thickness was measured by Vernier calipers immediately after injection.

Fifteen minutes later, paw thickness was measured again, and the mice were killed by decapitation. The hind paws of the mice were imaged, and paw tissues were collected, dried for 24 hours at 50°C, and weighed. Evans blue was extracted by 24-hour incubation in formamide at 50°C, and the OD values were read at 620 nm using a spectrophotometer. The concentration of Evans blue dye was determined based on the corresponding standard curve and expressed as ng/mg of tissue weight. The mice were initially treated with PBS or cromolyn sodium (25 mg/kg) for 3 days by intraperitoneal injection. On the fourth day, the mice were subjected to the above experiment.

#### **ELISA**

From  $1 \times 10^4$  to  $5 \times 10^4$  mast cells were incubated with test compound for 30 minutes before supernatant was collected. Supernatants were stored at  $-80^{\circ}$ C until used for ELISA. All data were normalized according to cell number. Histamine was detected with an ELISA Kit from Abcam (Cambridge, UK) according to manufacturer's instructions. Tryptase beta 2, serotonin, monocyte chemotactic protein 1 (MCP-1) and TNF- $\alpha$  were analyzed with ELISA kits from CUSABIO (Houston, Tex). Each dot represents an independent biological replicates from peritoneal mast cells (PMCs) isolated from >4 animals.

#### qRT-PCR

Total RNA was extracted from PMCs or hind paw tissues using TRIzol reagent (Takara Bio, Shiga, Japan), and the first-strand cDNA was reversely transcribed by using the RevertAid First Strand cDNA Synthesis Kit (Thermo Fisher Scientific). The cDNAs of the tested cytokines and chemokines were quantitated by quantitative RT-PCR (qRT-PCR) using the Bestar SybrGreen qPCR master mix reagent (DBI Bioscience, Newark, Del). The shown data represent the relative abundance of the indicated RNA normalized to that of GAPDH. The nucleic acid stain (Super GelRed, no. S-2001) was purchased from US Everbright Inc (Suzhou, China). The qRT-PCR primer sequences for the test cytokines and chemokines were shown in Table E1 in this article's Online Repository (available at <a href="https://www.jacionline.org">www.jacionline.org</a>). All qRT-PCR experiments were performed on an ABI 7500 system (Applied Biosystems, Thermo Fisher Scientific) according to the manufacturer's instructions.

#### Statistical analysis

The data are presented as the mean  $\pm$  SEM. Statistical comparisons were made with unpaired Student *t*-test, and differences were considered significant at P < .05.

#### **RESULTS**

### Preparation, structural features, and antimicrobial activity of the tick salivary peptide IPDef1

Because there have been some clinical cases of itch caused by the bites of hard ticks, we wondered whether the salivary peptide IPDef1 from the tick Ixodes persulcatus (Fig 1, A) can induce itching and scratching responses in mice. First, we chemically synthesized IP-R and then folded it by air oxidation in slightly alkaline Tris-HCl buffer. That oxidized product, IP-O was purified to homogeneity by RP-HPLC and was eluted at a retention time of 20.4 minutes, which was 1.4 minutes later than the reduced form was eluted (retention time, 19.0 minutes) (Fig 1, B), indicating that the reduced form and oxidized product of IP-Def1 have different polarities. This difference suggests that the formation of an intramolecular disulfide bond can decrease the polarity of this peptide. To verify disulfide bond formation, we analyzed the reduced form and oxidized product of IPDef1 using MALDI time-of-flight mass spectrometry. The results showed that the mass-to-charge ratios of IP-O and IP-R were 4195.1 and 4201.5, respectively (Fig 1, C). The measured molecular weight of IP-O was 4194.1 Da, which was 6.4 Da less than the

2240 LI ET AL J ALLERGY CLIN IMMUNOL

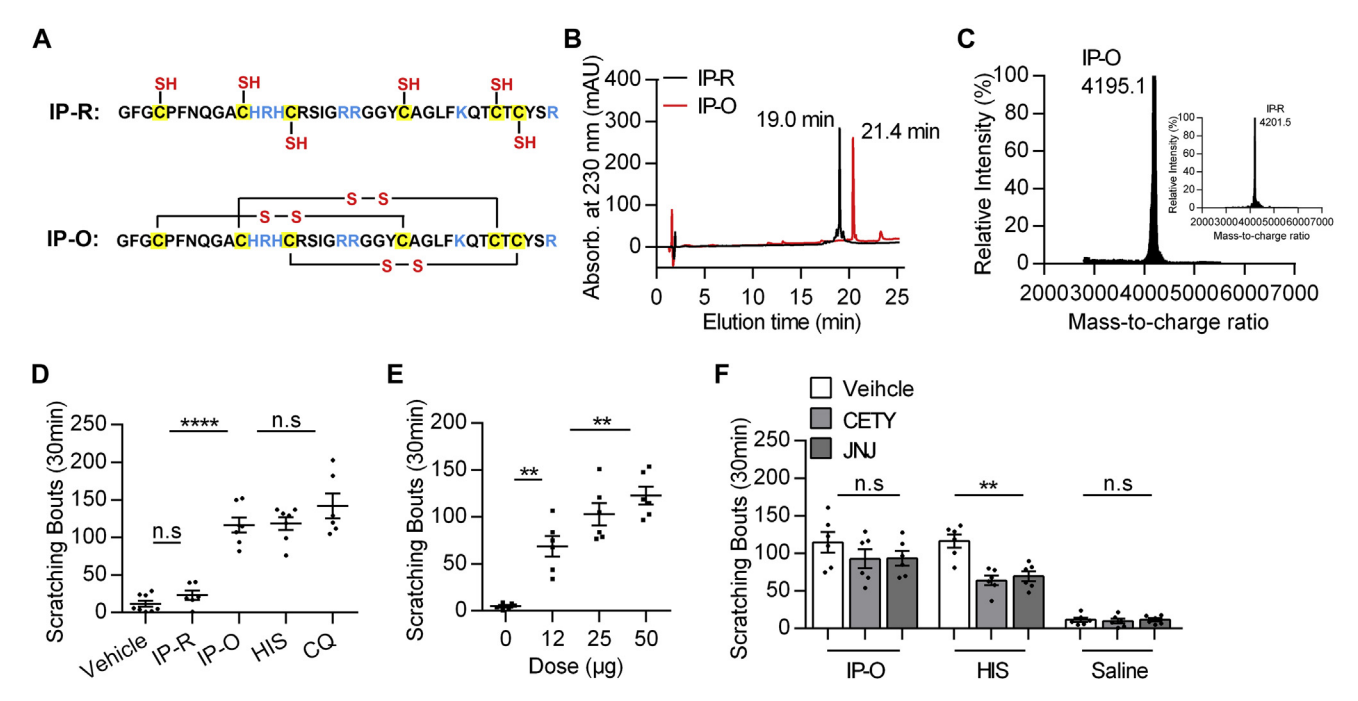


FIG 1. The tick peptide IPDef1 causes HIS-independent itch in mice. **A**, Amino acid sequence of the peptide IPDef1 from the tick *Ixodes persulcatus*. IP-R and IP-O are the reduced and oxidized forms of IPDef1, respectively. *SH* represents the thiol group of cysteine. The connectivity of disulfide bonds is indicated by the *solid line* with *S-S*. The cysteine residues are shaded in *yellow*, and the basic residues are displayed in *blue*. **B**, Oxidative refolding of chemically synthetic linear IPDef1. RP-HPLC shows the difference in retention time between IP-R and IP-O. **C**, MALDI time-of-flight mass spectrometry analysis of IP-R (*inset*) and IP-O. **D**, Scratching responses induced by intradermal injection of vehicle (saline, n = 8), IP-R (50  $\mu$ g, n = 6), IP-O (50  $\mu$ g, n = 7), HIS (10  $\mu$ mole, n = 7), and CQ (200  $\mu$ g, n = 9) in mice. **E**, Dose-dependent scratching responses induced by intradermal injection of vehicle (saline, n = 6), IP-O (12  $\mu$ g, n = 6), IP-O (25  $\mu$ g, n = 7), and IP-O (50  $\mu$ g, n = 6). **F**, Difference in scratching responses induced by intradermal injection of IP-O (25  $\mu$ g, n = 6), HIS (10  $\mu$ mole, n = 6), and saline in vehicle-treated (*white*), CETY-treated (*light gray*), and JNJ-treated mice (*dark gray*). Each *dot* represents an individual mouse. All data are presented as the mean  $\pm$  SEM. \*\*P < .01; \*\*\*\*P < .0001. *ns*, Not significant.

molecular weight of IP-R (4200.5 Da). These data indicate that 6 hydrogen atoms of the cysteines of the reduced peptide were removed when 3 disulfide bridges were formed. Additionally, analysis of circular dichroism indicated that IP-O displayed a minimum at 208 nm and a maximum at 198 nm (see Fig E1, A in this article's Online Repository at ww.jacionline.org), demonstrating that the reduced form of IPDef1 folds into a native-like conformation similar to that of other peptides with cysteinestabilized  $\alpha$ -helical and  $\beta$ -sheet structures. In contrast to that of IP-O, the secondary structure of IP-R was mainly dominated by irregular coils (Fig E1, A). The 3-dimensional structure of IPDef1 was modeled using the structure of the defensin mytilus galloprovincialis defensin-1 as a template (Protein Data Bank: 1FJN) with the SWISS-MODEL server. The predicted structure of IPDef1 had 1  $\alpha$ -helix domain at the N-terminus and 2  $\beta$ -sheet domains at the C-terminus (Fig E1, B).

As in representative invertebrate defensins, the connectivity of 3 disulfide bridges (Cys<sup>4</sup>-Cys<sup>25</sup>, Cys<sup>11</sup>-Cys<sup>33</sup>, and Cys<sup>15</sup>-Cys<sup>35</sup>) formed the core skeleton of IPDef1 (Fig E1, B). In addition, IPO presented nearly the same secondary structure in different solutions, including water, 0.9% sodium chloride, and PBS (Fig E1, C), suggesting that IP-O has a stable structure in different solutions. Because diverse bacteria are present in the habitats of ticks and because IPDef1 belongs to the ancient invertebrate-type defensin family and contains 6 disulfide-paired cysteines, we

performed MIC experiments to investigate the antimicrobial activities of IPDef1. IP-O effectively inhibited the growth of 5 tested standard gram-positive bacteria, exhibiting MIC values of 0.5 to 2  $\mu$ mol/L, whereas its reduced form, IP-R, showed much weaker bioactivity against these bacteria, showing MIC values of 6 to 16  $\mu$ mol/L (see Fig E2 in this article's Online Repository at www.jacionline.org). However, both forms of IPDef1 (IP-R and IP-O) did not seem to exert bioactivity against 2 tested standard gram-negative bacteria, exhibiting MIC values of >30  $\mu$ mol/L (Fig E2). These results suggest that only IP-O exerts excellent antibacterial effects against gram-positive bacteria. Additionally, the conformation of cysteine-stabilized  $\alpha$ -helical and  $\beta$ -sheet is closely related to the antimicrobial activity of IPDef1.

#### IPDef1 causes HIS-independent itch in mice

After preparing IPDef1, we examined whether the peptide can induce itching and scratching responses in mice. IP-R and IP-O were intradermally injected into the cheeks of mice, and IP-O but not IP-R elicited significant scratching behavior (vehicle, 11.7  $\pm$  4.0; IP-R, 23.17  $\pm$  6.1; IP-O, 116.6  $\pm$  9.9; P < .0001) (Fig 1, D). Moreover, IP-O induced scratching behavior in a dose-dependent manner (Fig 1, E). The best-characterized type of itch in humans and rodents, HIS-dependent itch, can be triggered by HIS.  $^{18}$  HIS is mainly secreted by skin mast cells and excites nearby sensory

fibers by acting on HIS receptors. 19 In our study, there was no significant difference in the total number of scratching bouts elicited by IP-O and that induced by HIS (IP-O, 116.6 ± 9.9; HIS,  $118.4 \pm 8.6$ ; P = .2) (Fig 1, D). These data suggest that IPDef1 probably has strong pruritogenic potential and that this potential may be dependent on its secondary structure. Considering that HIS induces pruritus in a HIS-dependent manner, <sup>20,21</sup> we wanted to know whether IP-O induces scratching responses in mice via a HIS-dependent pathway. HIS-induced itch can be almost completely blocked by HIS receptor H1/4 antagonists. The H1R antagonist cetirizine (CETY; 10 mg/kg)<sup>21</sup> and the H4R antagonist JNJ7777120 (JNJ; 40 mg/kg) were administered intraperitoneally 30 minutes prior to the injection of IP-O or HIS. Compared with vehicle (saline), CETY and JNJ significantly reduced HIS-induced scratching (vehicle, 116.5 ± 8.8; CETY,  $64.0 \pm 6.4$ ; P = .0007; JNJ,  $69.5 \pm 7.8$ ; P = .0017), but both failed to reduce IP-O-induced scratching behavior (vehicle,  $114.7 \pm 13.5$ ; CETY,  $92.6 \pm 12.6$ ; P = .2627; JNJ,  $93.5 \pm 8.8$ ; P = .2332) (Fig 1, F). These results suggest that IP-O may cause HIS-independent itch in mice. We selected another tick salivary peptide, IRDef2 from I ricinus, to determine the universal ability of tick salivary peptides to cause itch. <sup>22,23</sup> Consistently, compared with vehicle and the reduced form of IRDef2, the oxidized product of IRDef2 elicited significant scratching behavior (vehicle,  $7.2 \pm 2.0$ ; reduced form of IRDef2,  $15.0 \pm 2.0$ ; oxidized product of IRDef2, 69.7  $\pm$  5.5) (see Fig E3 in this article's Online Repository at www.jacionline.org).

### IP-O activates DRG neurons with extracellular Ca<sup>2+</sup> influx

To further investigate the neural mechanism underlying IP-Oinduced itch, we examined whether the peptide IP-O directly acts on mouse DRG neurons. Consistent with the behavioral data (Fig 1, D), IP-O but not IP-R induced a robust increase in  $[Ca^{2+}]_i$  in DRG neurons, exhibiting an EC<sub>50</sub> value of 2.45  $\pm$  0.68  $\mu$ mol/L (Fig 2, A-C); this finding indicates that IPDef1 directly acts on DRG neurons to evoke itch through a mechanism dependent on the proper folding of the secondary structure of the peptide. This increase in [Ca<sup>2+</sup>]<sub>i</sub> in cultured DRG neurons was also seen in representative Fura-2 ratiometric images showing IP-Revoked (10 µmol/L, white arrowheads) and IP-O-evoked (10 μmol/L, yellow arrowheads) responses (Fig 2, C). Notably, approximately 7% of the cultured mouse DRG neurons evoked by IP-O (10 μmol/L) exhibited a robust increase in [Ca<sup>2+</sup>]<sub>i</sub> in each experiment, which was similar to the percentage of DRG neurons that exhibited an increase in [Ca<sup>2+</sup>]<sub>i</sub> following treatment with CQ or BAM (IP-O,  $7.5 \pm 1.0\%$ ; CQ,  $6.8 \pm 0.9\%$ ; BAM,  $5.8 \pm 0.9\%$ ; P = .2413) (Fig 2, D). Previous studies have shown that some pruritogens, including CQ and BAM, mediate itch sensation through activating a highly restricted population of small-diameter neurons in the DRG. <sup>3,24,25</sup> In addition, the specific neurons that selectively detect itch-inducing chemicals and peptides comprise approximately 5% of all DRG neurons. These results suggest that the IP-O-evoked increase in [Ca<sup>2+</sup>]<sub>i</sub> seen in DRG cultures reflects the activation of a specific subset of DRG neurons, which may be the same population activated by CQ and/or BAM. We performed further experiments to characterize the increase in  $[Ca^{2+}]_i$  by extracellular  $Ca^{2+}$  influx or intracellular Ca<sup>2+</sup> store release in mouse DRG neurons. Extracellular Ca<sup>2+</sup> was found to be necessary for the increase in [Ca<sup>2+</sup>]<sub>i</sub> induced by IP-O and CQ, but not that induced by BAM, because the effects of these 2 substances were almost completely abolished in Ca<sup>2+</sup>-free bath solution (Fig 2, *E*). This result suggests that in the absence of extracellular Ca<sup>2+</sup>, IP-O and CQ, unlike BAM, did not mobilize Ca<sup>2+</sup> release from intracellular stores. However, IP-O, CQ, or BAM application in the presence of extracellular Ca<sup>2+</sup> triggered Ca<sup>2+</sup> influx across the plasma membrane (Fig 2, *E*). These data show that IP-O acts on DRG neurons and triggers the influx of Ca<sup>2+</sup> through transduction channels on the plasma membrane.

### Mouse MrgprC11 and human MRGPRX1 are the main itch receptors for IP-O on DRG neurons

IP-O directly acts on primary sensory neurons to evoke itch, and the proportion of IP-O-sensitive neurons among total DRG neurons is similar to the proportions of neurons activated by the 2 well-known MRGPR-dependent pruritogens CQ and BAM. Thus, it can be inferred that IP-O-induced itch is mediated by an MRGPR-dependent neural pathway. We cloned each of the 12 mouse Mrgpr genes that have been reported to be itch-related functional receptors into a mammalian expression vector and transfected them individually into HEK293T cells. By fusing green fluorescent protein to the C-terminus of the Mrgpr coding sequences, we were able to visualize the transfected cells and confirm the proper membrane localization of the receptors. Then, we examined the effects of IP-O on the 12 mouse *Mrgprs* by calcium imaging. The results showed that  $22.4 \pm 2.0\%$ MrgprA3-overexpressing HEK293T cells and 76.4 ± 2.0% MrgprC11-overexpressing HEK293T cells responded to IP-O (10 µmol/L). MrgprC11 conferred the strongest responses to the peptide, with an EC<sub>50</sub> value of 4.63  $\pm$  0.52  $\mu$ mol/L, whereas the other receptors conferred either weak or no responses to the peptide IP-O (MrgprA1, 2.0 ± 0.7%; MrgprA2, 4.0 ± 0.7%; MrgprA4, 6.4 ± 1.0%; MrgprA10, 1.0 ± 0.3%; MrgprA12,  $6.0 \pm 0.7\%$ ; MrgprA14,  $1.2 \pm 0.3\%$ ; MrgprA16,  $4.2 \pm 0.5\%$ ; MrgprA19,  $2.2 \pm 0.5\%$ ; MrgprB4,  $5.4 \pm 0.9\%$ ; MrgprB5,  $3.6 \pm 0.6\%$ ; P < .0001) (Fig 3, A-D; and see Fig E4 in this article's Online Repository at www.jacionline.org). In contrast, MrgprC11-overexpressing HEK293T cells exhibited nearly no response to IP-R (see Fig E5 in this article's Online Repository at www.jacionline.org), indicating that IPDef1 activates Mrgpr receptors through a mechanism dependent on the folding of its secondary structure. MrgprA3 and MrgprC11 were activated by their agonists CQ and BAM, respectively, confirming that they are functional receptors and are sensitive to IP-O (Fig 3, A and B). The main MRGPRXs of the human MRGPR family (MRGPRX1, X2, X3 and X4) are much smaller than those of the murine Mrgpr family. We examined the effects of IP-O on MRGPRXs and found that IP-O intensely activated MRGPRX1, exhibiting an EC<sub>50</sub> value of  $4.32 \pm 0.48 \,\mu$ mol/L. IP-O moderately activated MRGPRX2 but did not affect human MRGPRX3 or MRGPRX4 (MRGPRX1, 77.6 ± 2.8%; MRGPRX2, 28.2 ± 2.7%; MRGPRX3,  $6.0 \pm 0.7\%$ ; MRGPRX4,  $2.6 \pm 0.5\%$ ; P < .0001) (Fig 3, C and F-H; and see Fig E6 in this article's Online Repository at www.jacionline.org). Like MrgprC11overexpressing HEK293T cells, MRGPRX1-overexpressing HEK293T cells did not respond to IP-R (see Fig E7 in this article's Online Repository at www.jacionline.org). Some studies have shown that MRGPRX1/MrgprC11 is preferentially activated by peptides that terminate in Arginine-Glycine-Tyrosine or

2242 LI ET AL J ALLERGY CLIN IMMUNOL

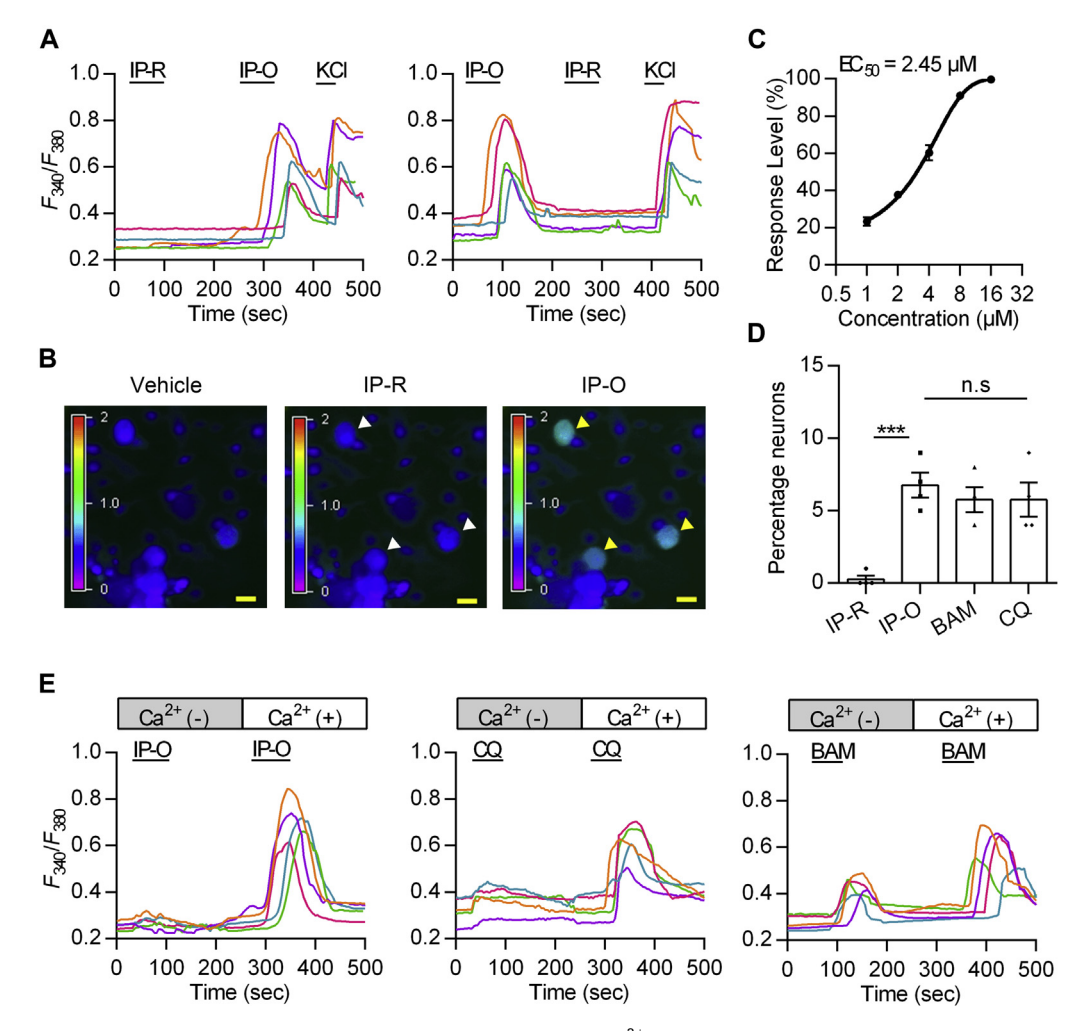


FIG 2. IP-O activates mouse DRG neurons with extracellular  $Ca^{2^+}$  influx. A, Representative calcium traces of cultured mouse DRG neurons in the presence of IP-R (10 μmol/L) and IP-O (10 μmol/L). B, Representative Fura-2 ratiometric images of IP-R–evoked (10 μmol/L, white arrowheads) and IP-O–evoked (10 μmol/L, yellow arrowheads) responses in cultured mouse DRG neurons. Bar = 20 μm. C, Dose-response curve of cultured mouse DRG neurons to IP-O (1, 2, 4, 8, and 16 μmol/L, respectively). n = 3 experiments/group. D, Percentage of cultured mouse DRG neurons that responded to IP-R (10 μmol/L), IP-O (10 μmol/L), BAM (50 μmol/L), and CQ (1 mmol/L). n = 3 experiments/group. All data are presented as the mean ± SEM. \*\*\*P < .001. ns, Not significant. E, Representative calcium traces of cultured mouse DRG neurons that responded to IP-O (10 μmol/L, left), CQ (1 mmol/L, middle), and BAM (50 μmol/L, right) in the absence and presence of extracellular calcium (2 mmol/L  $Ca^{2^+}$ ).

Arginine-Phenylalanine-amide.  $^{26,27}$  Given that IP-O does not terminate with either motif, these results suggest that IP-O represents a completely new type of ligand for MRGPRX1/MrgprC11. In addition, like the endogenous ligand BAM, IP-O has the highest affinity for the itch receptors MrgprC11 and MRGPRX1 (MrgprC11,  $76.4 \pm 2.0\%$ ; MRGPRX1,  $77.6 \pm 2.8\%$ ) (Fig 3, C and G), indicating that the molecular mechanism of IP-O-induced itch may be similar to that of BAM.

Coimmunoprecipitation was also used to determine whether the peptide IP-O directly interacts with the tested mouse and human MRGPRs. The peptide His-IP, which contains IPDef1 fused to a 6-histidine (His) residue tag at the N-terminus, was chemically synthesized and oxidatively refolded according to the procedure described for the peptide IP-O above (see Fig E8 in this article's Online Repository at www.jacionline.org). HEK293T cells were transfected with a plasmid expressing an N-flag-tagged mouse Mrgpr (MrgprC11 or A3) or human MRGPR (MRGPRX1,

X2, X3, or X4). The results of coimmunoprecipitation showed that both mouse MrgprC11 and MrgprA3 directly interacted with the peptide IP-O (see Fig E9, *A* in this article's Online Repository at www.jacionline.org). Furthermore, human MRGPRX1 and MRGPRX2 but not MRGPRX3 and MRGPRX4 directly interacted with the peptide IP-O (Fig E9, *B*).

To further investigate the role that MrgprC11 plays in IP-O-induced itch, MrgprC11 knockout C57BL/6 mice were generated by the CRISPR/Cas9 approach (see Fig E10 in this article's Online Repository at www.jacionline.org). Then, we compared IP-O-evoked Ca<sup>2+</sup> signals in DRG neurons isolated from MrgprC11-deficient mice to those in DRG neurons isolated from wild-type (WT) littermates and found that Ca<sup>2+</sup> signals evoked by IP-O were significantly attenuated in MrgprC11-deficient DRG neurons compared with WT DRG neurons (Fig 3, *I*). Moreover, BAM-evoked responses were also attenuated in MrgprC11-deficient neurons compared with WT neurons. These

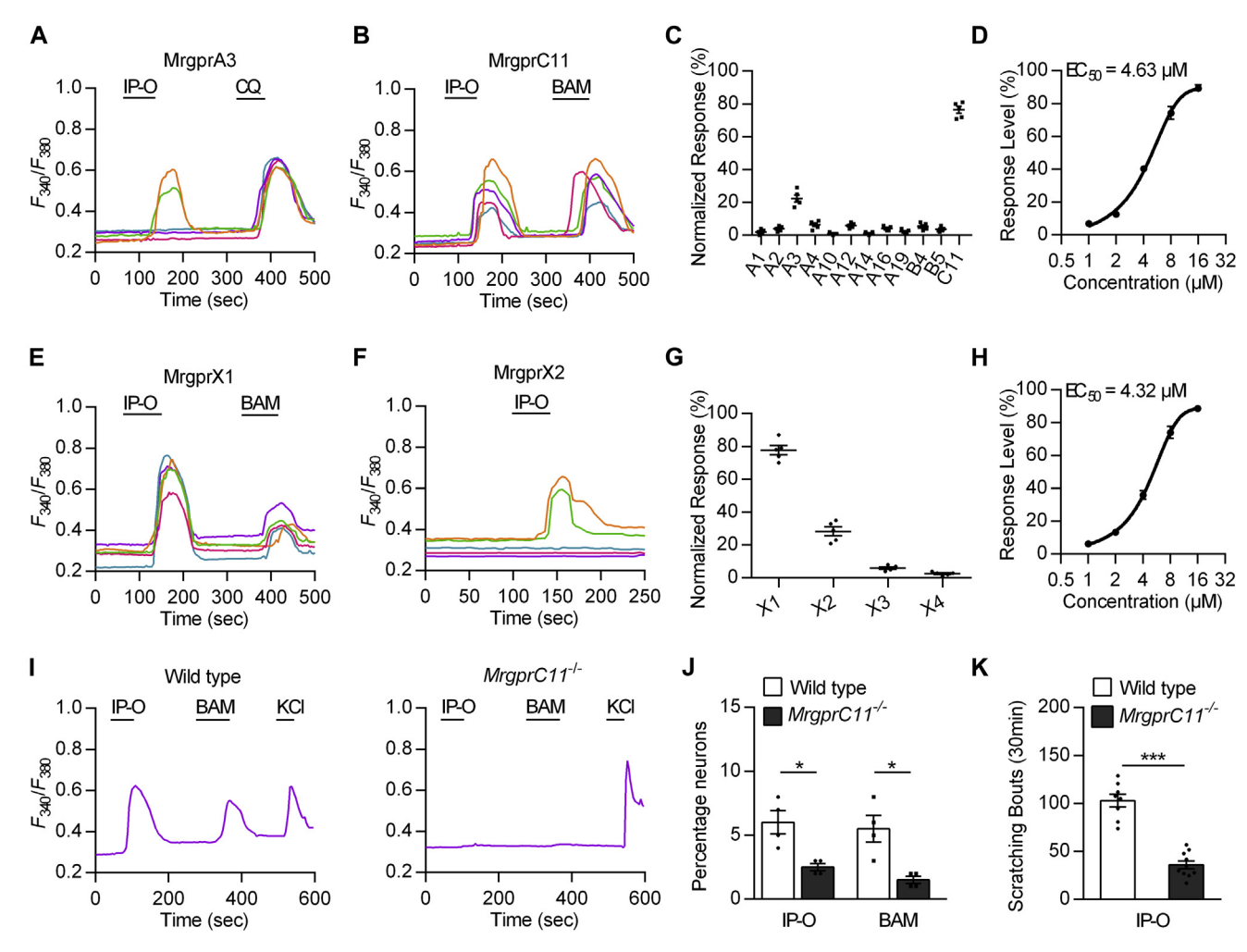


FIG 3. Mouse MrgprC11 and human MRGPRX1 are 2 itch receptors for IP-O. A and B, Representative calcium traces showing the responses of mouse MrgprA3 and MrgprC11 expressed on HEK293T cells to IP-O (10 μmol/L). C, Percentage of 12 mouse Mrgprs (MrgprA1, A2, A3, A4, A10, A12, A14, A16, A19, B4, B5, and C11) expressed on HEK293T cells that responded to IP-O. n = 5 experiments/group. D, Doseresponse curve for MrgprC11 expressed on HEK293T cells to IP-O (1, 2, 4, 8, and 16 μmol/L). n = 3 experiments/group. E and F, Representative calcium traces showing the responses of human MRGPRX1 and MRGPRX2 expressed on HEK293T cells to IP-O (10 μmol/L). G, Percentage of human MRGPRS (MRGPRX1, X2, X3, and X4) expressed on HEK293T cells that responded to IP-O. n = 5 experiments/group. H, Doseresponse curve for MRGPRX1 expressed on HEK293T cells to IP-O (1, 2, 4, 8, and 16 μmol/L, respectively). n = 3 experiments/group. I, Representative calcium response traces of WT (*left*) and *MrgprC11*<sup>-/-</sup> (*right*) mouse DRG neurons exposed to IP-O (10 μmol/L), BAM (50 μmol/L), and KCI (50 mmol/L), respectively. J, Prevalence of IP-O and BAM sensitivity in WT (*white*) and *MrgprC11*<sup>-/-</sup> DRG neurons (*black*). n = 4 experiments/group. K, Difference in scratching responses induced by intradermal injection of IP-O (25 μg) in WT (*white*, n = 8) and *MrgprC11*<sup>-/-</sup> mice (*black*, n = 10). All data are presented as the mean ± SEM. \*P < .05; \*\*\* P < .05; \*\*\* P < .001.

results suggest that MrgprC11 is the key neuroreceptor for both IP-O and BAM. Compared with those isolated from WT mice, the cultured DRG neurons isolated from MrgprC11-deficient mice showed a decrease in the proportion of IP-O-sensitive neurons (Fig 3, J). A similar decrease in the percentage of BAM-sensitive neurons was observed in DRG neurons isolated from MrgprC11-deficient mice compared with those isolated from WT mouse DRG neurons (Fig 3, J). To further investigate the *in vivo* role of MrgprC11 in IP-O-induced itch, we evaluated the itching responses induced by IP-O in MrgprC11-deficient mice. As expected, the scratching response induced by IP-O were dramatically alleviated in MrgprC11-deficient mice

compared with those of WT mice (Fig 3, K). Together, these data indicate that MrgprC11 is the main itch receptor for IP-O on mouse DRG neurons and plays a key role in IP-O-induced itch.

## TRPV1 is the downstream ion channel coupled to IP-O-activated MrgprC11/MRGPRX1 on DRG neurons

Mouse MrgprC11 and human MRGPRX1 were identified as the main receptors for the peptide IP-O. However, the signaling pathway and ion channel downstream of IP-O are unknown. It has **2244** LI ET AL

been observed that many G protein-coupled receptors on DRG neurons transduce signals via TRP channels. 28,29 TRPV1expressing afferents mediate responses to a variety of pruritogens, and TRPV1-deficient mice display reduced responses to HIS.<sup>30</sup> CQ and BAM activate a subset of TRPV1-positive neurons.31 These findings suggest that TRPV1 is a likely candidate transduction channel in MRGPR pruritic pathways that should not be ignored. Accordingly, we used live-cell calcium imaging to examine the overlap between the sensitivity of WT mouse DRG neurons to IP-O and the TRPV1 agonist Cap. AMG9810, an inhibitor of TRPV1, severely attenuated the effect of IP-O (10 μmol/L) on WT mouse DRG neurons (Fig 4, A). After washout, IP-O induced a relatively normal increase in  $[Ca^{2+}]_i$  (Fig 4, A). Subsequent exposure to Cap (1 µmol/L) produced a further increase in  $[Ca^{2+}]_i$  in all IP-O-positive cells (Fig 4, A). These data indicate that TRPV1 is likely involved in the signaling pathway associated with IP-O-induced itch. We then compared IP-O-evoked Ca<sup>2+</sup> signals in DRG neurons isolated from TRPV1-deficient mice to those in DRG neurons isolated from WT littermates and found that Ca2+ signals evoked by IP-O were significantly attenuated in TRPV1-deficient DRG neurons compared with WT DRG neurons (Fig 4, B). As expected, Capevoked responses were also attenuated in TRPV1-deficient neurons compared with WT neurons, but the TRPA1 agonist AITC evoked Ca<sup>2+</sup> signals in both TRPV1-deficient and WT DRG neurons (Fig 4, B). These results indicate that IP-O-activated DRG neurons express both TRPV1 and TRPA1, whereas TRPV1 but not TRPA1 is required for the IP-O-evoked signaling pathway. Cultured DRG neurons isolated from TRPV1-deficient mice showed a decrease in the proportion of IP-O-sensitive neurons compared with that exhibited by WT mouse DRG neurons (Fig 4, C). A similar decrease in the proportion of IP-O-sensitive neurons was observed in WT mouse DRG neurons treated with the TRPV1 antagonist AMG9810 (Fig 4, C). Furthermore, there was a significant reduction in the proportion of HIS-sensitive cells in the DRG from TRPV1-deficient mice and AMG9810-treated DRG neurons from WT mice compared with that in WT DRG neurons (Fig 4, C). These findings are consistent with the previous finding that TRPV1 is required for HIS signaling in sensory neurons. 32 In contrast, the number of CQ-responsive cells was similar in WT mouse DRG neurons, AMG9810-treated WT mouse DRG neurons, and  $Trpv1^{-/-}$  mouse DRG neurons (Fig 4, C), indicating that TRPV1 is not required for CQ signaling, which is consistent with the findings of a previous study.<sup>29</sup> In addition, we evaluated the itching responses induced by these 3 substances in TRPV1deficient mice. Similar to that evoked by HIS, the scratching response induced by IP-O was significantly alleviated in TRPV1-deficient mice compared with in WT mice (Fig 4, D). There was no significant difference in the total number of scratching bouts induced by CQ over a period of 30 minutes between TRPV1-deficient and WT mice (Fig 4, D). Thus, our results indicate that the functional TRPV1 channel is required for IP-Oevoked DRG activation and IP-O-induced itch in mice.

Consistent with this conclusion, calcium imaging indicated that Cap but not IP-O affected the Ca<sup>2+</sup> response of mouse TRPV1 expressed in heterologous HEK293T cells (see Fig E11, *A* in this article's Online Repository at www.jacionline.org). Whole-cell patch-clamp recordings showed that the peptide IP-O did not affect the currents of TRPV1-overexpressing HEK293T cells (Fig E11, *B*). Furthermore, coimmunoprecipitation experiments showed that the peptide IP-O did not directly

interact with TRPV1 channels (Fig E11, C). All these results suggest that the peptide IP-O is not a direct agonist of TRPV1.

### TRPA1 is not required for MrgprC11/X1-mediated DRG neuron activation by IP-O

Although TRPV1 is required for IP-O-evoked Ca<sup>2+</sup> signals, it does not mediate all forms of itch. TRPA1, which is highly expressed in a subset of TRPV1-positive neurons, is activated by a number of pain-producing compounds, including isothiocyanates.<sup>33</sup> In addition, TRPA1 is activated downstream of some G protein-coupled receptors. Thus, we further examined whether there is an overlap between the sensitivity of WT mouse DRG neurons to IP-O and the TRPA1 agonist AITC. HC-030031, an antagonist of the TRPA1 channel, 34 had little effect on IP-Oevoked Ca<sup>2+</sup> signals in DRG neurons from WT mice (Fig 5, A). We then compared IP-O-evoked Ca<sup>2+</sup> signals in DRG neurons isolated from TRPA1-deficient mice to those isolated from WT littermates. The results indicated that IP-O-evoked Ca<sup>2+</sup> signals were similar in TRPA1-deficient and WT DRG neurons (Fig 5, B). In addition, the TRPV1 agonist Cap induced similar Ca<sup>2+</sup> signals in both TRPA1-deficient and WT DRG neurons, whereas AITCevoked responses were significantly attenuated in TRPA1deficient DRG neurons compared with in WT DRG neurons (Fig 5, B). These data indicate that TRPA1 is unlikely to be involved in the IP-O signaling pathway. Both DRG neurons isolated from TRPA1-deficient mice and AMG9810-treated DRG neurons isolated from WT mice showed similar responses to IP-O as DRG neurons isolated from WT mice (Fig 5, C). Likewise, no difference was observed in the proportion of HIS-sensitive neurons among these 3 kinds of DRG neurons (Fig 5, C). In contrast, the proportion of CQ-sensitive neurons among cultured neurons isolated from TRPA1-deficient mice was decreased compared with that among neurons isolated from WT mice (Fig 5, C). Similar results were observed for WT neurons treated with the TRPA1 antagonist HC-030031 (Fig 5, C). These findings show that TRPA1 is required for CQ signaling in sensory neurons. In contrast, the numbers of CO-responsive cells among WT mouse neurons, AMG9810-treated WT mouse neurons, and mutant neurons were similar (Fig 5, C), indicating that TRPV1 is not required for CQ signaling. These results were completely consistent with the finding of a previous report.<sup>35</sup> Furthermore, we evaluated the itching responses induced by IP-O, HIS, and CQ in TRPA1-deficient mice. No significant difference in the total number of scratching bouts induced by IP-O over a period of 30 minutes, which was similar to that induced by HIS, was found between TRPA1-deficient and WT mice (Fig 5, D). However, the scratching response induced by CQ in TRPA1-deficient mice was significantly alleviated compared with that in WT mice.

Correspondingly, the results of the calcium imaging experiment indicated that AITC but not IP-O activated mouse TRPA1 expressed on heterologous HEK293T cells (see Fig E12, *A* in this article's Online Repository at www.jacionline.org). Whole-cell patch-clamp recordings showed that the peptide IP-O did not affect the currents of the TRPA1 channel overexpressed in HEK293T cells (Fig E12, *B*). Moreover, coimmunoprecipitation experiments showed that the peptide IP-O did not directly interact with the ion channel TRPA1 (Fig E12, *C*). Taken together, our results indicate that TRPA1 is not required for IP-O–evoked excitation of DRG neurons or subsequent IP-O–induced itch in mice.

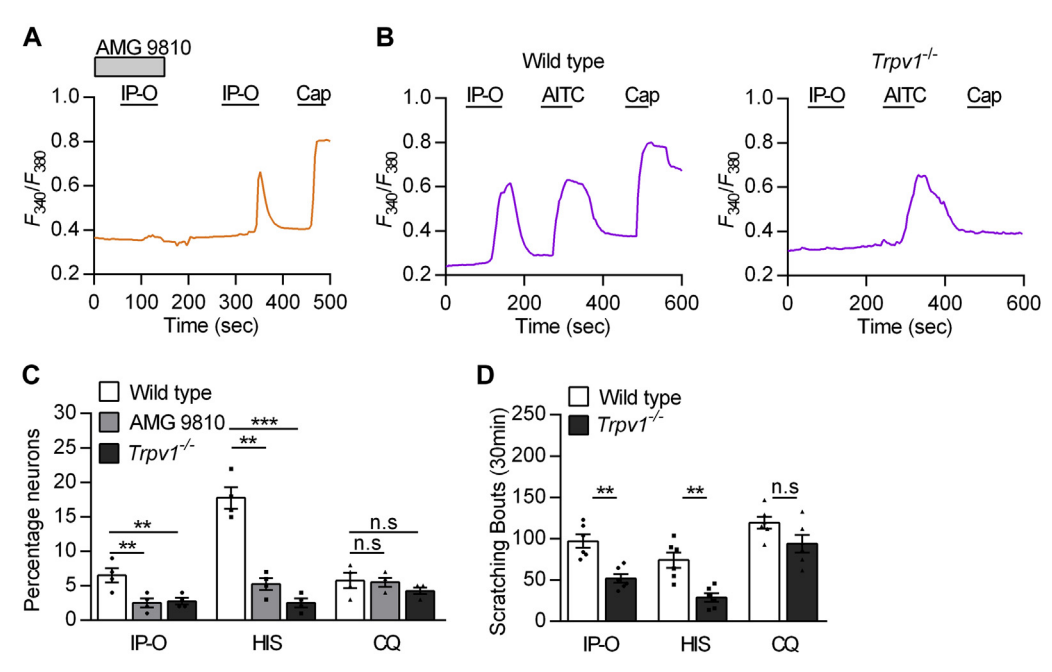


FIG 4. TRPV1 is the downstream ion channel that mediates IP-O–evoked DRG neuron activation and IP-O–induced itch in mice. **A**, Representative calcium traces of WT DRG neurons exposed to IP-O (10 μmol/L) following pretreatment (3 minutes) with or without AMG9810 (50 μmol/L). **B**, Representative calcium traces of WT (*left*) and  $Trpv1^{-/-}$  (*right*) DRG neurons exposed to IP-O (10 μmol/L) followed by AITC (100 μmol/L) and Cap (1 μmol/L). **C**, Prevalence of IP-O, HIS (1 μmol/L), and CQ (1 mmol/L) sensitivity in WT (*white*), AMG9810-treated WT DRG (50 μmol/L, *gray*), and  $Trpv1^{-/-}$  DRG neurons (*black*). n = 4 experiments/group. **D**, Difference in scratching responses induced by intradermal injection of IP-O (25 μg, n = 6), HIS (10 μmole, n = 6), and CQ (200 μg, n = 6) in WT mice (*white*) and  $Trpv1^{-/-}$  mice (*black*). All data are presented as the mean  $\pm$  SEM. \*\*P < .01; \*\*\*P < .01;

### IP-O activates mast cells through MrgprB2 and induces acute inflammation in mice

The above results show that IP-O evokes itch by directly activating MrgprC11/X1 to regulate downstream TRPV1 on pruriceptors and that the MrgprC11/X1-TRPV1 pathway is an important signaling pathway for IP-O-induced itch. However, we found that IP-O moderately activated human MRGPRX2 (an ortholog of mouse MrgprB2) (Fig 3, G) selectively expressed on mast cells but not on primary sensory neurons. It is possible that some mast cell-derived mediators, such as proteases and 5-hydroxy tryptamine, are involved in IP-O-induced itch. Therefore, we examined the effect of IP-O on mouse MrgprB2 by calcium imaging as described above. The results showed that some MrgprB2-overexpressing HEK293T cells responded to IP-O (Fig 6, A). We also found that IP-O directly activated PMCs isolated from mice (Fig 6, B). Sodium cromoglicate (cromolyn), a mast cell stabilizer, can effectively inhibit granule release. We evaluated the itching responses induced by IP-O, PAMP9-20, and anti-IgE in cromolyn-treated mice. In contrast to the scratching responses induced by PAMP9-20 and anti-IgE, there was no significant difference in the total number of scratching bouts induced by IP-O over a period of 30 minutes between cromolyn-treated and vehicle-treated mice (Fig 6, C). It is likely that mast cells activated by IP-O made little contribution to itching and had unknown effects in mice. Evans blue extravasation assays showed that intraplantar injection of IP-O induced acute inflammation in mice (Fig 6, D and E). We measured paw thickness of the mice before and after IP-O treatment and found that the paw thickness was significantly increased after the injection of IPO (see Fig E13 in this article's Online Repository at www. jacionline.org). In addition, compared with that in vehicle-treated mice, acute inflammation induced by IP-O was reduced in cromolyn-treated mice (Fig 6, F).

The activation of mast cells by intraplantar injection of IP-O caused acute inflammation in mice, but it was unclear which mediators released from mast cells were required for this effect. We detected in vitro release of HIS, serotonin, tryptase β2, TNF- $\alpha$ , and MCP-1 from mouse PMCs on stimulation by IP-O (12, 25, or 50  $\mu$ mol/L), PAMP (100  $\mu$ mol/L), and anti-IgE (25  $\mu$ g/mL). Compared with vehicle, IP-O resulted in the releases of HIS, serotonin, and tryptase β2 (Fig 6, G-I). In addition, IP-O also induced the releases of TNF- $\alpha$  and MCP-1 with a moderate increase (see Fig E14 in this article's Online Repository at www.jacionline.org). These mediators released from mast cells may have an effect on recruiting immune cells and facilitating the progress of inflammation. Furthermore, we analyzed the mRNA expression of more cytokines and chemokines in IP-O-treated PMCs. Among the test cytokine and chemokine genes, no significant change was observed at the level of mRNA expression after IP-O stimulation in PMCs (see Fig E15 in this article's Online Repository at www.jacionline.org), which was consistent with the degranulation release of mast cells. Taken together, these results suggest that IP-O activates mast cells through MrgprB2/X2 and induces acute inflammation but that mast cell activation appears to make little contribution to IP-O-induced itch.

2246 LI ET AL

J ALLERGY CLIN IMMUNOL

JUNE 2021

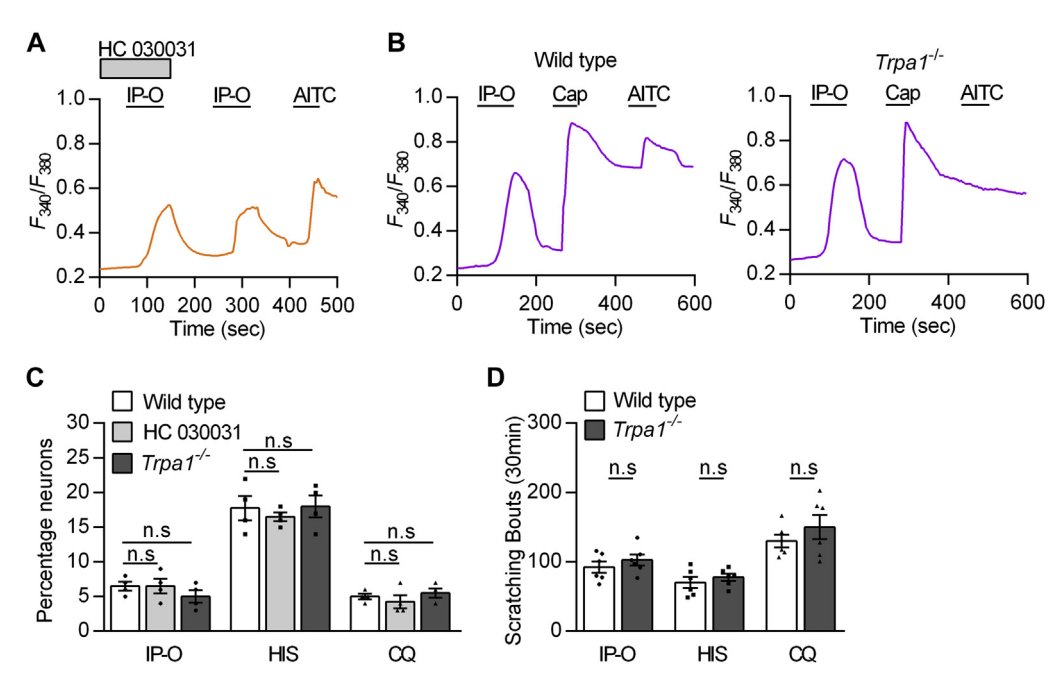


FIG 5. TRPA1 is not required for IP-O–evoked DRG neuron activation or IP-O–induced itch in mice. **A**, Representative calcium traces of WT DRG neurons exposed to IP-O (10  $\mu$ mol/L) following pretreatment (3 minutes) with or without the HC030031 (500  $\mu$ mol/L). **B**, Representative calcium traces of WT (*left*) and  $Trpa1^{-/-}$  (*right*) DRG neurons exposed to IP-O (10  $\mu$ mol/L) followed by Cap (1  $\mu$ mol/L) and AITC (100  $\mu$ mol/L). **C**, Prevalence of IP-O, HIS (1  $\mu$ mol/L), and CQ (1  $\mu$ mol/L) sensitivity in WT (*white*), HC030031-treated WT (500  $\mu$ mol/L, *light gray*), and  $Trpa1^{-/-}$  DRG neurons (*dark gray*). n = 4 experiments/group. **D**, Difference in scratching responses induced by intradermal injection of IP-O (25  $\mu$ g, n = 6), HIS (10  $\mu$ mole, n = 6), and CQ (200  $\mu$ g, n = 6) in WT (*white*) and  $Trpa1^{-/-}$  mice (*dark gray*). All data are presented as the mean  $\pm$  SEM.

#### **DISCUSSION**

As vectors of various pathogens, ticks commonly induce skin pruritus by biting humans and animals. Which class of substance causes scratching and itching following a tick bite: the carried pathogens or endogenous components expressed by ticks? We postulated that endogenous components of ticks are most likely responsible for itch induction for 2 reasons. First, dogs bitten by the tick *O brasiliensis* exhibit continuous and intense itching behavior, but typical tick-borne pathogens are not detected in the sera of bitten dogs. <sup>10</sup> Tick bites with and without pathogens both lead to skin pruritus in dogs. Second, many arthropod bites and stings can cause itching behavior, but ants, bees, spiders, and scorpions have not yet been found to transmit pathogens.

We found that 2 tick salivary defensin peptides, IPDef1 and IRDef2, significantly induced itching and scratching behavior in mice on intradermal injection. Defensins in the saliva of ticks were discovered to act as new pruritogenic agents, at least partially explaining the pathological phenomenon of skin pruritus caused by tick bites. Defensins in the saliva of ticks share high homology and structural similarity with ancient invertebrate defensins. Thus, we found a new large class of pruritogenic peptide agents that is completely different from previously reported pruritogenic peptides such as  $BAM^{24}$  and mouse/human  $\beta$ -defensins.  $^{36,37}$  Our findings provide many new molecular probes and tools for studying itch receptors.

Interestingly, our study revealed that the tick salivary peptide IPDef1 exerts 2 activities through 2 different signaling pathways in mice: MrgprC11/X1-mediated DRG neuron activation and MrgprB2/X2-mediated mast cell activation. First, IPDef1 triggers

DRG neuron activation by specifically acting on MrgprC11/X1 on DRG neurons and induces cellular calcium influx into DRG neurons through the downstream TRPV1 channel, which causes itching in mice. Second, IPDef1 also activates mast cells through MrgprB2/X2, a recently discovered membrane receptor on mast cells that induces acute inflammation in mice. Besides taking part in the pathology and mortality caused by envenomation, mast cells were previously found to play an important role in detoxification of harmful poisons. Mast cell degranulation releases CPA3 and chymase and reduces the toxicity of animal venoms (such as those of scorpions, bees, and snakes) by degrading their venom peptides. <sup>38,39</sup> It is still unclear whether IPDef1 induces mast cells to release CPA3 or chymase for detoxification by activating MrgprB2/X2.

Coimmunoprecipitation, calcium imaging, genetic ablation, and behavior experiments revealed the molecular mechanism by which the peptide IPDef1 directly interacts with Mrgprs (mainly MrgprC11/X1) and activates DRG neurons to induce itch. However, this mechanism is not related to the HIS signaling pathway. We not only found a class of new pruritogenic peptide agents responsible for arthropod bite- or sting-induced itch but also revealed the related neural mechanisms, laying the foundation for the development of anti-itch drugs to combat arthropod bite- or sting-induced pruritus. Moreover, an inhibitor of TRPV1 was shown to specifically block calcium influx into DRG neurons activated by the tick peptide IPDef1 and inhibit the pruritus induced by IPDef1 in cell and animal behavior experiments. TRPV1 is a promising target of anti-itch drugs, and its inhibitors are potential candidates for preventing and treating the pruritus

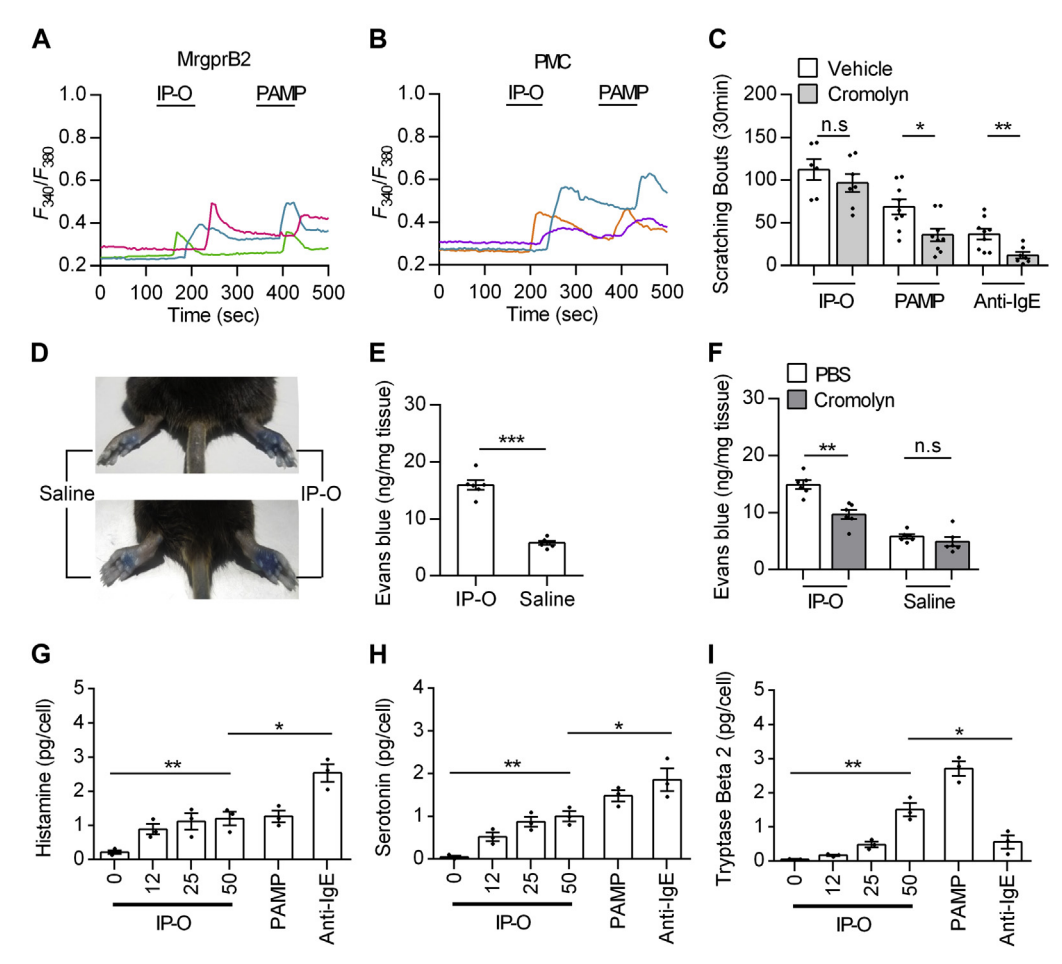


FIG 6. IP-O activates mast cells through MrgprB2 and induces acute inflammation in mice. A, Representative calcium traces of mouse MrgprB2-overexpressing HEK293T cells to IP-O (10  $\mu$ mol/L). B, Representative calcium traces of isolated mouse PMCs to IP-O (10  $\mu$ mol/L). C, Difference in scratching responses induced by intradermal injection of IP-O (25  $\mu$ g, n = 7), PAMP (25  $\mu$ g, n = 10), and anti-IgE (1  $\mu$ g, n = 9) in vehicle-treated (saline, white) or cromolyn-treated mice (light gray). D, Representative images of Evans blue extravasation 15 minutes after intraplantar injection of saline (5  $\mu$ L, left paw) or IP-O (5  $\mu$ L, 2 mg/mL, right paw). n = 6. E, Quantification of Evans blue content in the paws after injection of saline or IP-O. F, Quantification of Evans blue content in the paws after injection of saline or IP-O in PBS-treated and cromolyn-treated mice. G to I, In vitro release of HIS (G), serotonin (H), and tryptase  $\beta$ 2 (I) from mouse PMCs on stimulation by IP-O (12, 25, 50  $\mu$ mol/L) or PAMP (100  $\mu$ mol/L) or anti-IgE (25  $\mu$ g/mL) or vehicle alone (IP-O = 0  $\mu$ mol/L). Each dot represents an independent biological replicate from PMCs isolated from >4 animals. All concentrations n = 3. All data are presented as the mean  $\pm$  SEM. \*P < .05; \*\*P < .01; \*\*\*P < .001.

induced by tick bites. Coincidentally, Li et al reported a case of a man bitten by the tick *L persulcatus* on Yunmeng Mountain in Beijing, China. The patient subsequently developed topical edematous erythema and itching, but oral antihistamine and topical calamine lotion did not improve his itching symptoms. This observation suggests that antihistamine drugs do not have an effect against pruritus induced by tick bites, providing evidence that tick bite–induced pruritus is independent of the HIS-related pathway. In short, our study identifies potential therapeutic targets and drugs for the prevention and treatment of pruritus induced by the bites or stings of arthropods such as ticks, mites, fleas, mosquitoes, bees, wasps, spiders, and scorpions.

The generation of peptides that induce itch resulted from the interaction between and coevolution of parasites and hosts or prey and predators. We speculate that there are 2 possible driving forces of this phenomenon. First, the generation of itchiness is a self-alarm and self-defense mechanism in hosts or predators. Itch

helps hosts or predators scratch away external threats. It is easily understood that hosts or predators evolve to produce itching signals against arthropod bites or stings. Second, the salivary or venom glands of these arthropods have evolved to produce peptides that induce pruritus, which are their molecular weapons for predation and defense, to attack hosts, protect against enemies, or deter competitors. 41 During long-term evolution, multiple peptide and protein families have been recruited to the animal salivary or venom systems. 42 Defensins have also been recruited to animal saliva and venoms as chemical weapons for predation and defense. Defensins belong to a class of ancient cationic peptides that are widely distributed in fungi, plants, and animals and are effector molecules of the innate immune system, exhibiting broad-spectrum antimicrobial activity against a range of bacteria and viruses. 43 Consistent with our finding that the ancient invertebrate defensin IPDef1 from the tick I persulcatus evokes itch by directly activating MrgprC11/X1 expressed on DRG neurons,

2248 LI ET AL J ALLERGY CLIN IMMUNOL

mouse and human  $\beta$ -defensins have also been identified as pruritogens that activate MRGPRs or TLR4. These results suggest that ancient invertebrate defensins were recruited early to the tick salivary systems and innovated a new toxicological function of itch induction. Our study not only reveals a new toxicological effect and mechanism of defensins in saliva or venoms but also brings to light a new link between neurobiology and immunology.

We thank Dr Qin Liu (Washington University School of Medicine, St Louis, Mo) for kindly providing plasmids of mouse MrgprA3 and MrgprC11. We also thank Drs Qin Liu and Dr Weishan Yang (Washington University School of Medicine, St Louis, Mo) for their valuable communications with us.

#### Key messages

- Two tick salivary peptides IPDef1 and IRDef2 induce itch in mice via a HIS-independent pathway.
- IPDef1 evokes itch by activating MrgprC11/X1 to sensitize downstream TRPV1 on DRG neurons.
- IPDef1 activates MrgprB2/X2 on mast cells to cause acute inflammation.

#### REFERENCES

- Cevikbas F, Lerner EA. Physiology and pathophysiology of itch. Physiol Rev 2020;100:945-82.
- 2. Lay M, Dong X. Neural mechanisms of itch. Annu Rev Neurosci 2020;43:187-205.
- Liu Q, Tang ZX, Surdenikova L, Kim S, Patel KN, Kim A, et al. Sensory neuronspecific GPCR Mrgprs are itch receptors mediating chloroquine-induced pruritus. Cell 2009;139:1353-65.
- Feng J, Luo JL, Yang P, Du JH, Kim BS, Hu HZ. Piezo2 channel-Merkel cell signaling modulates the conversion of touch to itch. Science 2018;360:530.
- Hoogstraal H, Gallagher M. Blisters, pruritus, and fever after bites by the Arabian tick Ornithodoros (Alectorobius) muesebecki. Lancet 1982;320:288-9.
- Jones AV, Tilley M, Gutteridge A, Hyde C, Nagle M, Ziemek D, et al. GWAS of self-reported mosquito bite size, itch intensity and attractiveness to mosquitoes implicates immune-related predisposition loci. Hum Mol Genet 2017;26:1391-406.
- Cyranoski D. East Asia braces for surge in deadly tick-borne virus. Nature 2018; 556;282-3.
- Holding M, Dowall S, Hewson R. Detection of tick-borne encephalitis virus in the UK. Lancet 2020;395:411.
- Fisher EJ, Mo J, Lucky AW. Multiple pruritic papules from lone star tick larvae bites. JAMA Dermatol 2006;142:491-4.
- Reck J, Soares JF, Termignoni C, Labruna MB, Martins JR. Tick toxicosis in a dog bitten by *Ornithodoros brasiliensis*. Vet Clin Pathol 2011;40:356-60.
- Cao Z, Yu Y, Wu Y, Hao P, Di Z, He Y, et al. The genome of Mesobuthus martensii reveals a unique adaptation model of arthropods. Nat Commun 2013;4:2602.
- Luo L, Li B, Wang S, Wu F, Wang X, Liang P, et al. Centipedes subdue giant prey by blocking KCNQ channels. Proc Natl Acad Sci U S A 2018;115:1646-51.
- Yang S, Yang F, Wei N, Hong J, Li B, Luo L, et al. A pain-inducing centipede toxin targets the heat activation machinery of nociceptor TRPV1. Nat Commun 2015;6: 2207
- Lin King JV, Emrick JJ, Kelly MJS, Herzig V, King GF, Medzihradszky KF, et al. A cell-penetrating scorpion toxin enables mode-specific modulation of TRPA1 and pain. Cell 2019;178:1362-74.e16.
- Osteen JD, Herzig V, Gilchrist J, Emrick JJ, Zhang C, Wang X, et al. Selective spider toxins reveal a role for the Nav1.1 channel in mechanical pain. Nature 2016; 534:494-9.
- Meng L, Xie Z, Zhang Q, Li Y, Yang F, Chen Z, et al. Scorpion potassium channelblocking defensin highlights a functional link with neurotoxin. J Biol Chem 2016; 291:7097-106
- Thangamani S, Wikel SK. Differential expression of Aedes aegypti salivary transcriptome upon blood feeding. Parasit Vectors 2009;2:34.
- Ikoma A, Steinhoff M, Ständer S, Yosipovitch G, Schmelz M. The neurobiology of itch. Nat Rev Neurosci 2006;7:535-47.

 Thurmond RL, Kazerouni K, Chaplan SR, Greenspan AJ. Antihistamines and itch. Handb Exp Pharmacol 2015;226:257-90.

- MeiXiong J, Dong XZ. Mas-related G protein-coupled receptors and the biology of itch sensation. Ann Rev Genet 2017;51:103-21.
- Wooten M, Weng HJ, Hartke TV, Borzan J, Klein AH, Turnquist B, et al. Three functionally distinct classes of C-fibre nociceptors in primates. Nat Commun 2014;5:4122.
- Chrudimská T, Slaninová J, Rudenko N, Růžek D, Grubhoffer L. Functional characterization of two defensin isoforms of the hard tick *Ixodes ricinus*. Parasit Vectors 2011:4:63.
- 23. Rudenko N, Golovchenko M, Grubhoffer L. Gene organization of a novel defensin of *Ixodes ricinus*: first annotation of an intron/exon structure in a hard tick defensin gene and first evidence of the occurrence of two isoforms of one member of the arthropod defensin family. Insect Mol Biol 2007;16:501-7.
- Lembo PM, Grazzini E, Groblewski T, O'Donnell D, Roy MO, Zhang J, et al. Proenkephalin A gene products activate a new family of sensory neuron-specific GPCRs. Nat Neurosci 2002;5:201-9.
- Sikand P, Dong XZ, LaMotte RH. BAM8–22 peptide produces itch and nociceptive sensations in humans independent of histamine release. J Neurosci 2011;31:7563.
- Han SK, Dong XZ, Hwang JI, Zylka MJ, Anderson DJ, Simon MI. Orphan G
  protein-coupled receptors MrgA1 and MrgC11 are distinctively activated by
  RF-amide-related peptides through the Gαq/11 pathway. Proc Natl Acad Sci U S
  A 2002:99:14740.
- Grazzini E, Puma C, Roy MO, Yu XH, Donnell D, Schmidt R, et al. Sensory neuron-specific receptor activation elicits central and peripheral nociceptive effects in rats. Proc Natl Acad Sci U S A 2004;101:7175.
- Jordt SE, Bautista DM, Chuang HH, McKemy DD, Zygmunt PM, Högestätt ED, et al. Mustard oils and cannabinoids excite sensory nerve fibres through the TRP channel ANKTM1. Nature 2004;427:260-5.
- Wilson SR, Gerhold KA, Bifolck-Fisher A, Liu Q, Patel KN, Dong XZ, et al. TRPA1 is required for histamine-independent, Mas-related G protein-coupled receptor-mediated itch. Nat Neurosci 2011;14:595-602.
- Valtcheva MV, Davidson S, Zhao CS, Leitges M, Gereau RW. Protein kinase C8
  mediates histamine-evoked itch and responses in pruriceptors. Mol Pain 2015;
  11:1.
- Imamachi N, Park GH, Lee HS, Anderson DJ, Simon MI, Basbaum AI, et al. TRPV1-expressing primary afferents generate behavioral responses to pruritogens via multiple mechanisms. Proc Natl Acad Sci U S A 2009;106:11330.
- Immke DC, Gavva NR. The TRPV1 receptor and nociception. Semin Cell Dev Biol 2006;17:582-91.
- McNamara CR, Mandel-Brehm J, Bautista DM, Siemens J, Deranian KL, Zhao M, et al. TRPA1 mediates formalin-induced pain. Proc Natl Acad Sci U S A 2007;104: 13525
- Yin SJ, Luo JL, Qian AH, Du JH, Yang Q, Zhou ST, et al. Retinoids activate the irritant receptor TRPV1 and produce sensory hypersensitivity. J Clin Invest 2013; 123:3941-51.
- Ru F, Sun H, Jurcakova D, Herbstsomer RA, MeiXong J, Dong X, et al. Mechanisms of pruritogen-induced activation of itch nerves in isolated mouse skin. J Physiol 2017;595:3651-66.
- Zhang L, McNeil BD. Beta-defensins are proinflammatory pruritogens that activate Mrgprs. J Allergy Clin Immunol 2019;143:1960-2.e5.
- 37. Feng J, Luo JL, Mack MR, Yang P, Zhang F, Wang G, et al. The antimicrobial peptide human beta-defensin 2 promotes itch through Toll-like receptor 4 signaling in mice. J Allergy Clin Immunol 2017;140:885-8.e6.
- 38. Akahoshi M, Song CH, Piliponsky AM, Metz M, Guzzetta A, Abrink M, et al. Mast cell chymase reduces the toxicity of Gila monster venom, scorpion venom, and vasoactive intestinal polypeptide in mice. J Clin Invest 2011;121:4180-91.
- Metz M, Piliponsky AM, Chen CC, Lammel V, Abrink M, Pejler G, et al. Mast cells can enhance resistance to snake and honeybee venoms. Science 2006;313: 526-30.
- Liu YH, Fang K, Wang HW, Han YH, Zhou HY. A case of tick bite by *Ixodes per-sulcatus*. J Clin Dermatol 31, 2002:720-720. [Chinese].
- Casewell NR, Wüster W, Vonk FJ, Harrison RA, Fry BG. Complex cocktails: the evolutionary novelty of venoms. Trends Ecol Evol 2013;28:219-29.
- Undheim EA, Jones A, Clauser KR, Holland JW, Pineda SS, King GF, et al. Clawing through evolution: toxin diversification and convergence in the ancient lineage Chilopoda (centipedes). Mol Biol Evol 2014;31:2124-48.
- Schneider T, Kruse T, Wimmer R, Wiedemann I, Sass V, Pag U, et al. Plectasin, a fungal defensin, targets the bacterial cell wall precursor Lipid II. Science 2010; 328:1168-72.

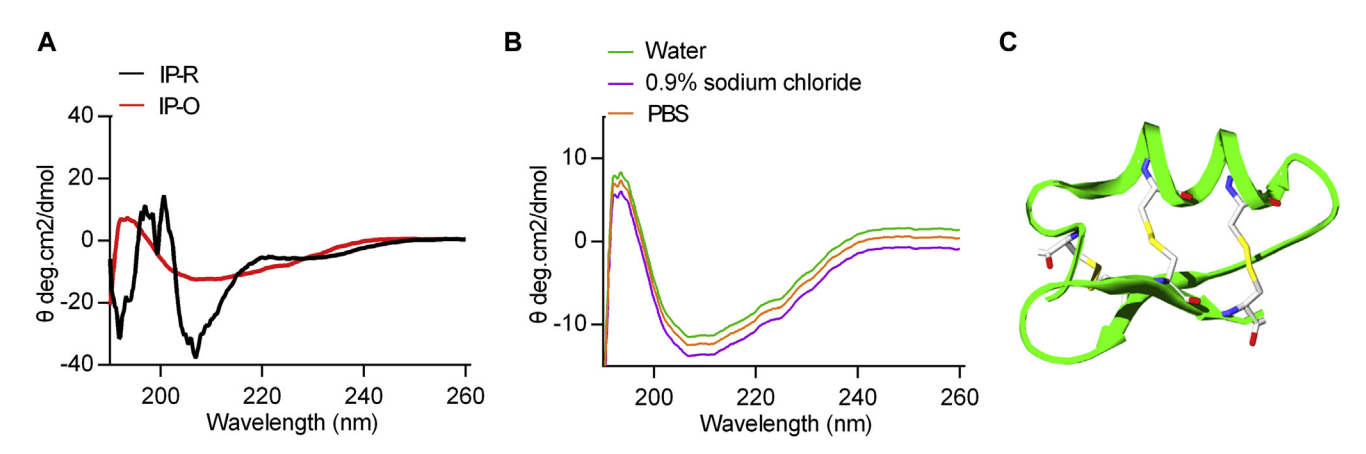


**FIG E1.** Structural features of the peptide IPDef1 from the tick *Ixodes persulcatus*. **A,** Secondary structure analysis of the reduced (IP-R) and oxidated (IP-O) forms of IPDef1. Circular dichroism spectrum shows structure difference between IP-R and IP-O. **B,** Secondary structure analysis of IP-O in different solutions. **C,** The homologous model of IPDef1. The 3-dimensional structure of IPDef1 is shown as a *solid ribbon* model and 3 disulfide bonds are displayed as a *line ribbon*. Diagram was generated using SWISS-MODEL.

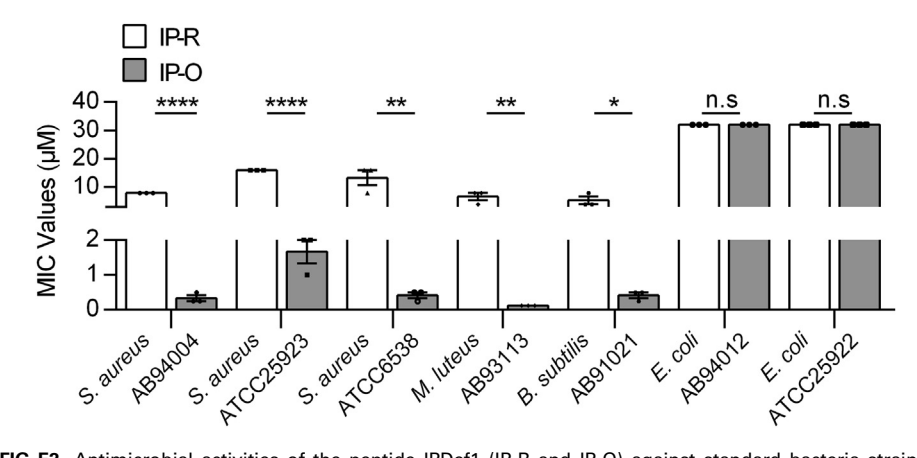


**FIG E2.** Antimicrobial activities of the peptide IPDef1 (IP-R and IP-O) against standard bacteria strains. The y-axis shows MIC values of IP-R and IP-O against 5 gram-positive bacteria and 2 gram-negative bacteria. \*P < .05; \*\*P < .01; \*\*\*\*P < .001.

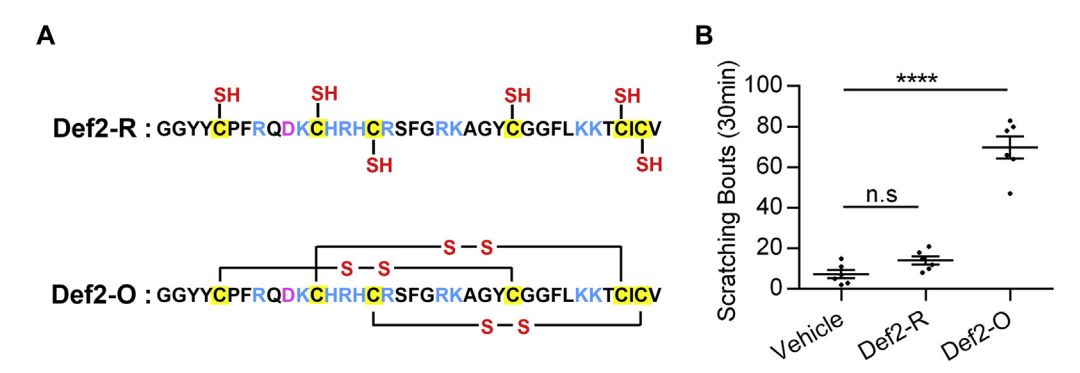


**FIG E3.** The tick salivary peptide IRDef2 induces itch responses in mice. **A**, Amino acid sequence of the peptide IRDef2 from the tick *I ricinus* saliva. Def2-R and Def2-O are the reduced and oxidated forms of IRDef2, respectively. *SH* represents the thiol group of cysteine. The connection mode of disulfide bond is displayed in a solid line with *S-S*. The cysteine residues are shaded with *yellow*, acidic residues are displayed in *pink*, and basic residues are displayed in *blue*. **B**, Scratching responses induced by intradermal injection of vehicle (saline), Def2-R (25  $\mu$ g) and Def2-O (25  $\mu$ g) in mice. Each *dot* represents an individual mouse. All groups n = 6. All data are presented as mean  $\pm$  SEM. \*\*\*\*\*P<.0001.

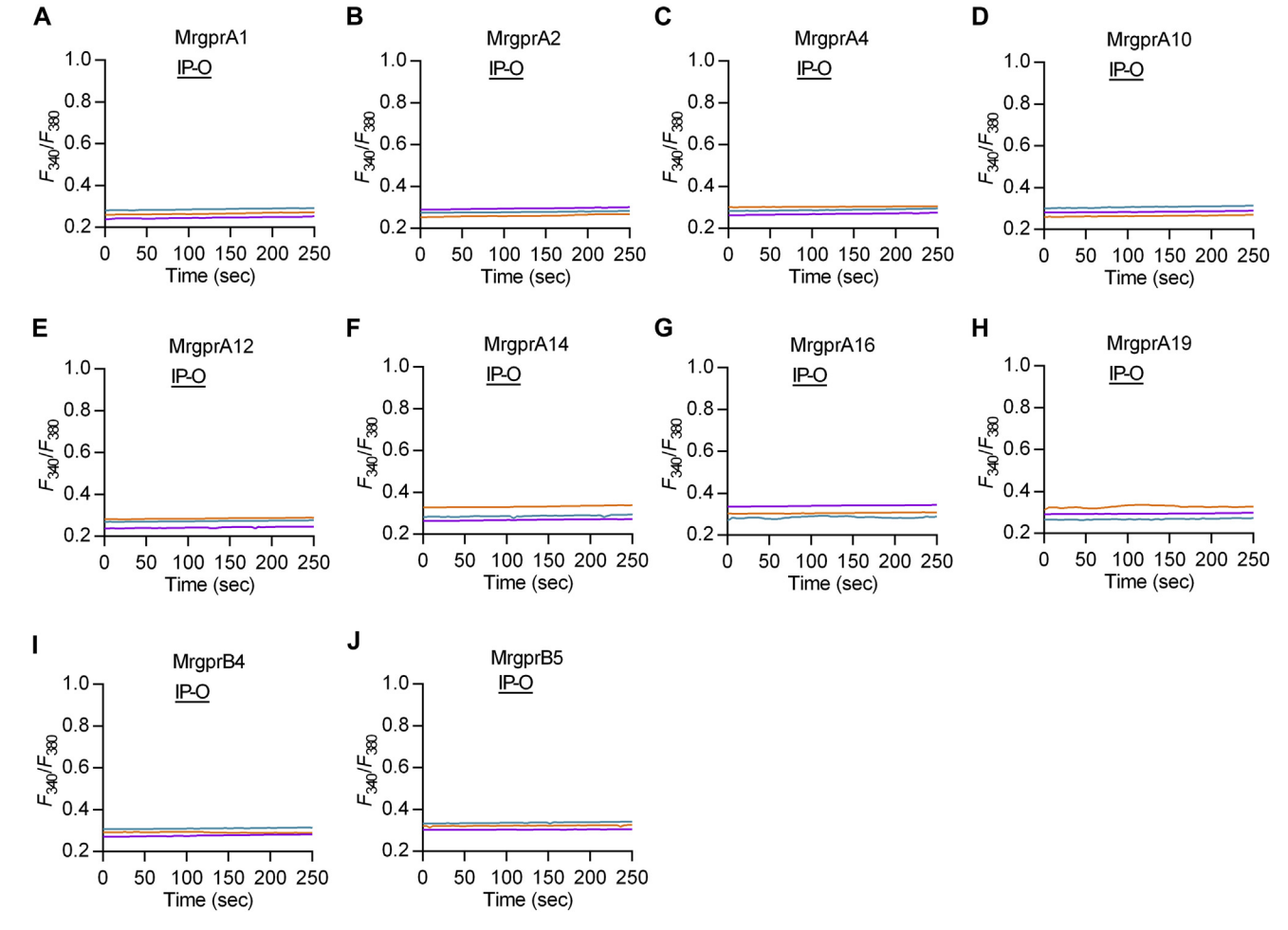


**FIG E4.** IP-O fails to activate mouse MrgprA1, A2, A4, A10, A12, A14, A16, A19, B4, and B5. **A to J**, Representative calcium traces of mouse Mrgprs (MrgprA1, A2, A4, A10, A12, A14, A16, A19, B4, and B5) expressed on HEK293T cells to IP-O (10  $\mu$ mol/L). n = 3 experiments/group.

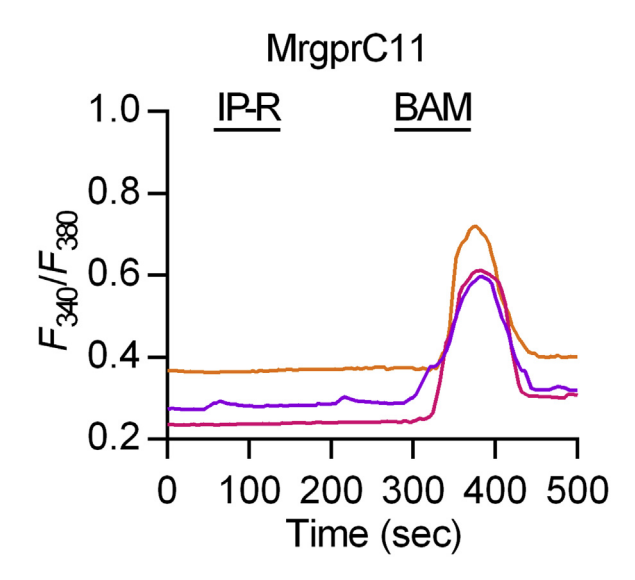
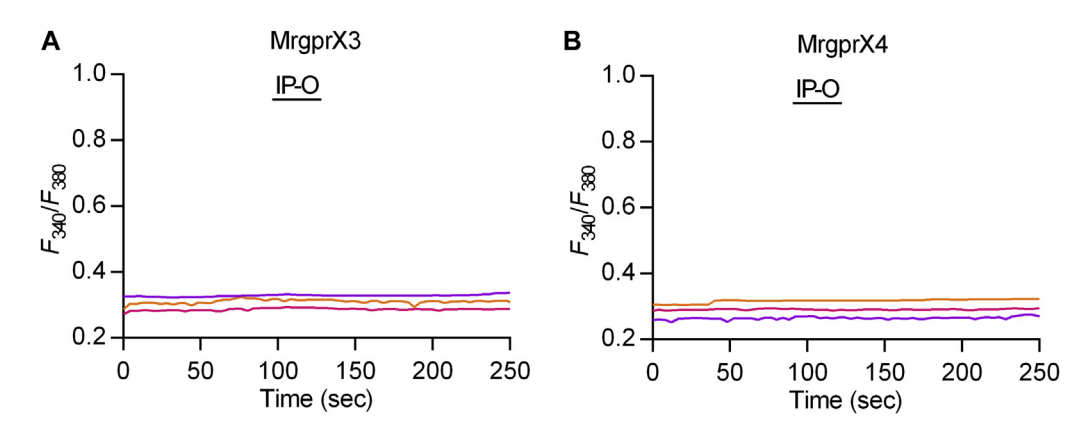


FIG E5. IP-R fails to activate mouse MrgprC11. Representative calcium traces of mouse MrgprC11 expressed on HEK293T cells to IP-R (10  $\mu mol/L)$ .



**FIG E6.** IP-O fails to activate human MRGPRX3 and MRGPRX4. **A and B,** Representative calcium traces of human MRGPRX3 and MRGPRX4 expressed on HEK293T cells to IP-O (10  $\mu$ mol/L). n = 3 experiments/group.

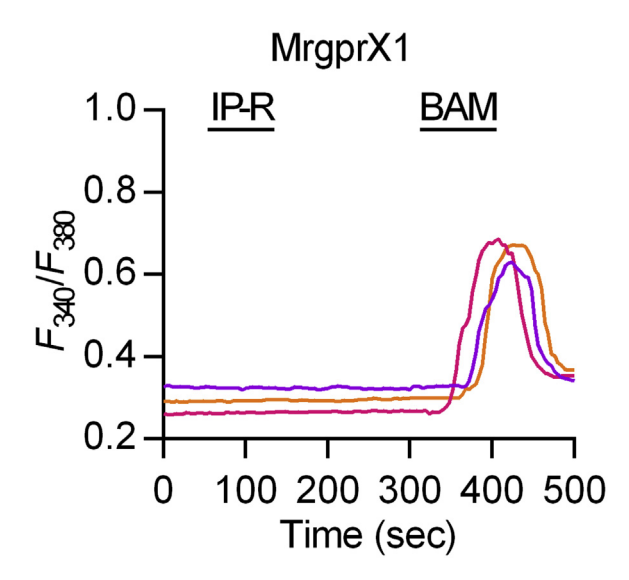


FIG E7. IP-R fails to activate human MRGPRX1. Representative calcium traces of human MRGPRX1 expressed on HEK293T cells to IP-R (10  $\mu$ mol/L).

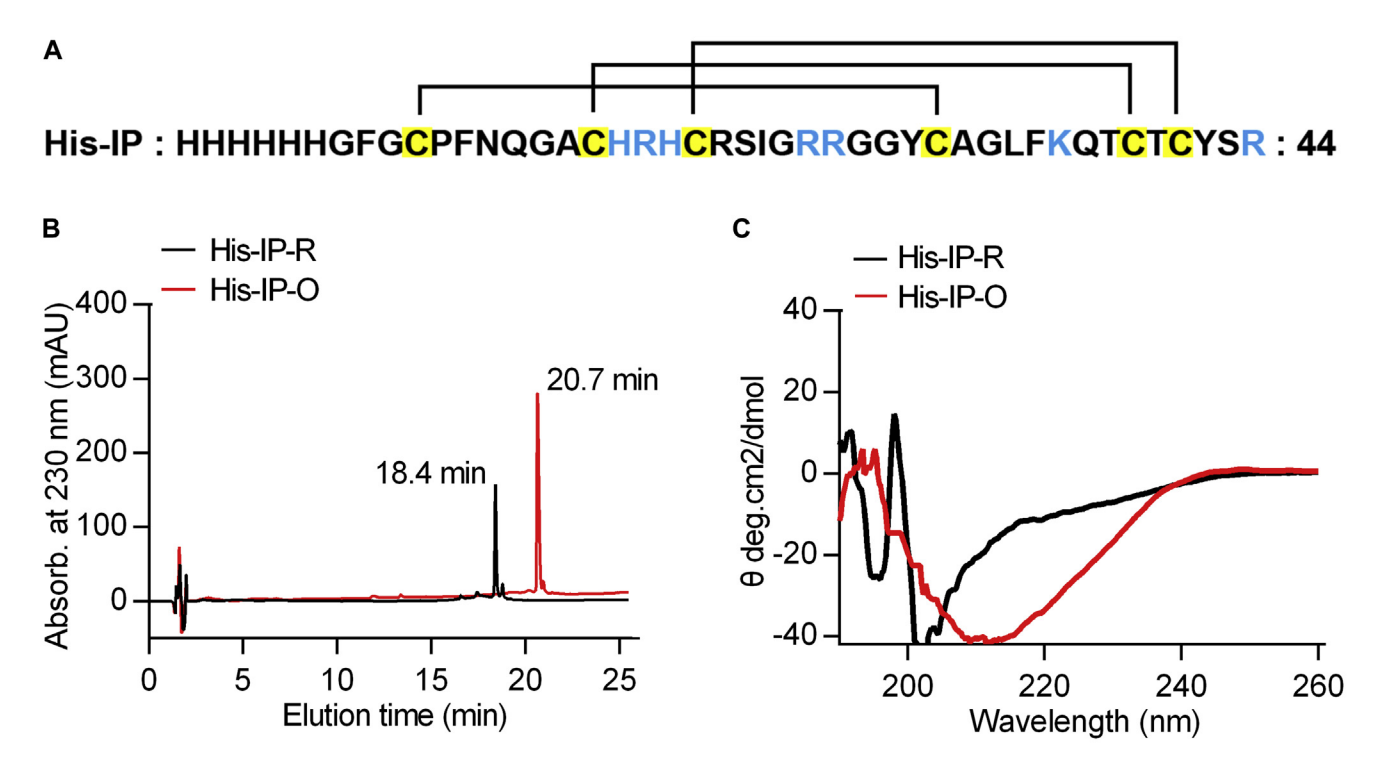


FIG E8. Preparation and structural feature of the peptide His–IP-O. A, Amino acid sequence of the peptide fused with His-IP. The connection mode of disulfide bond is displayed in a *solid line*. Cysteine residues are shaded with *yellow*, and basic residues are displayed in *blue*. B, Oxidative refolding of chemically synthetic His-IP. RP-HPLC shows retention time difference between the reduced (His–IP-R) and oxidated (His–IP-O) peptides. C, Secondary structure analysis of His-IPDef1. Circular dichroism spectrum shows structure difference between His–IP-R and His–IP-O.

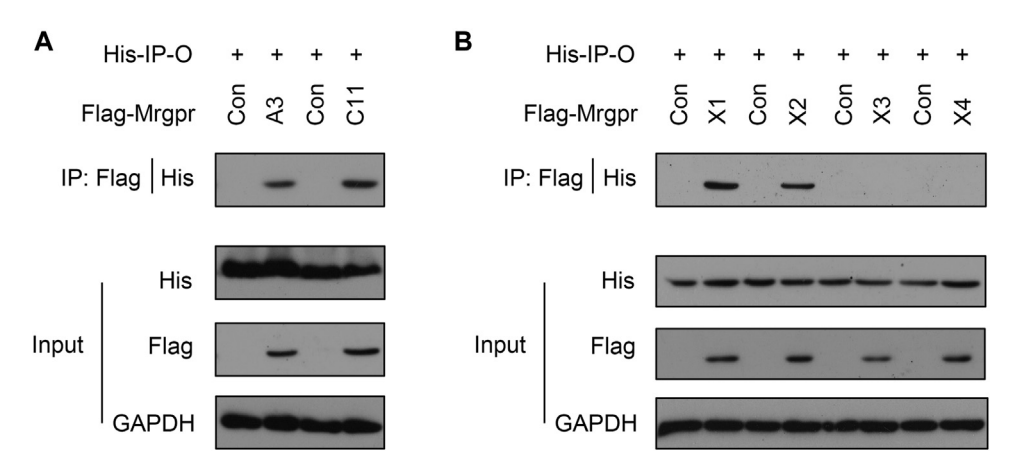
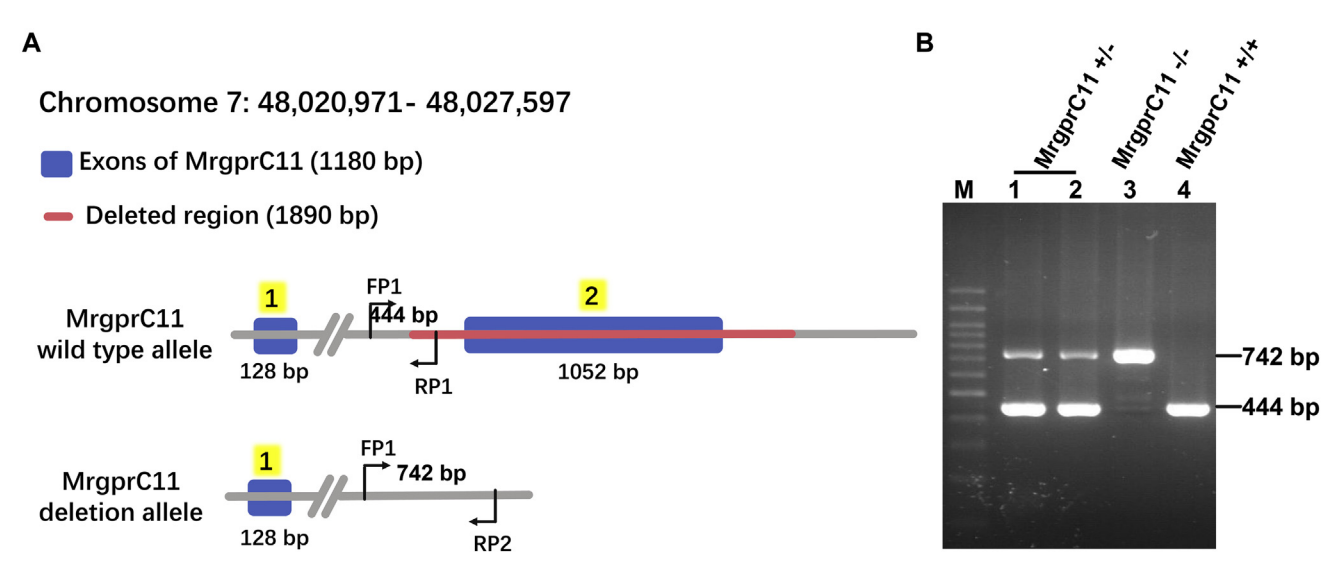
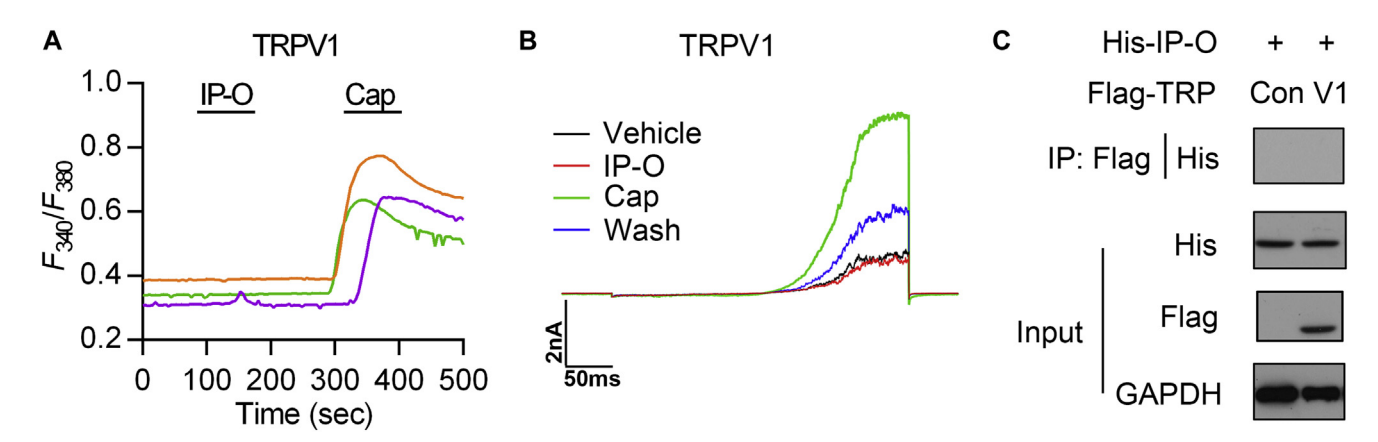


FIG E9. IP-O directly interacts with mouse MrgprA3/C11 and human MRGPRX1/X2. A and B, Coimmunoprecipitation analysis of the peptide IP-O with the mouse MrgprA3/C11 and human MRGPRX1-X4. HEK293T cells were transfected with the plamid pcDNA3.1 expressing different N-flag-tagged mouse Mrgprs (MrgprA3 and C11) (A) and human MRGPRs (MRGPRX1, X2, X3 and X4) (B), respectively.



**FIG E10.** Creation of MrgprC11 knockout mice by CRISPR/Cas9. **A and B,** Strategy and genotyping results of MrgprC11 knockout mouse. *FP1*, Forward primer 1; *RP1*, reverse primer 1.



**FIG E11.** IP-O fails to interact with TRPV1 directly. **A,** Representative calcium traces of TRPV1 expressed on HEK293T cells to IP-O (10  $\mu$ mol/L). **B,** Effect of IP-O on the current of TRPV1-overexpressing HEK293T cells. **C,** Coimmunoprecipitation analysis of the peptide IP-O with the mouse TRPV1. *Con,* Control represents HEK293T cells transfected with the plamid pcDNA3.1-Flag.

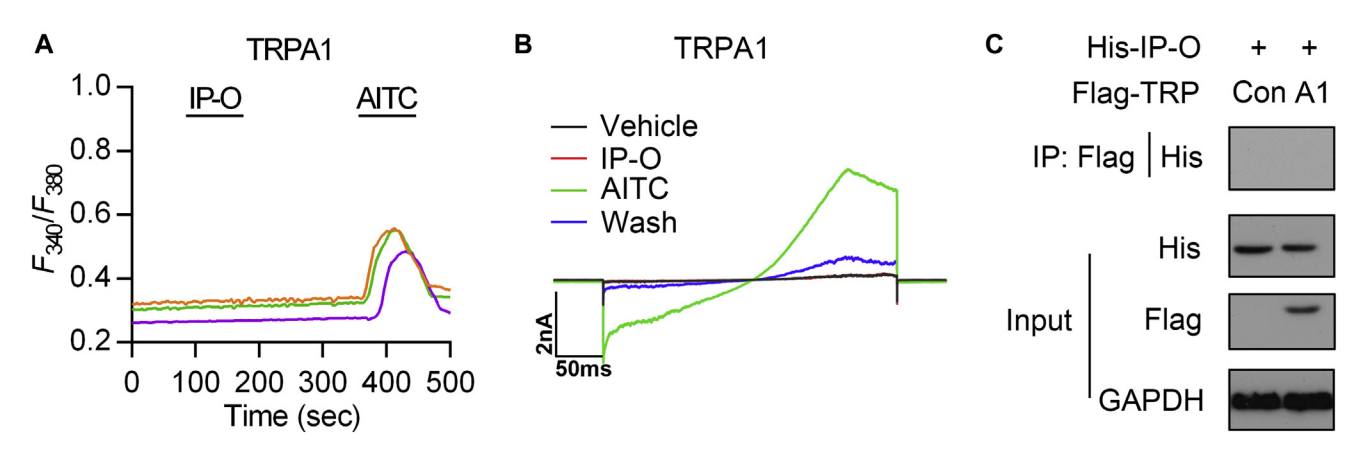


**FIG E12.** IP-O fails to interact with TRPA1 directly. **A,** Representative calcium traces of TRPA1-overexpressing HEK293T cells to IP-O (10  $\mu$ mol/L). **B,** Effect of IP-O on the current of TRPA1-overexpressing HEK293T cells. **C,** Coimmunoprecipitation analysis of the peptide IP-O with the mouse TRPA1.

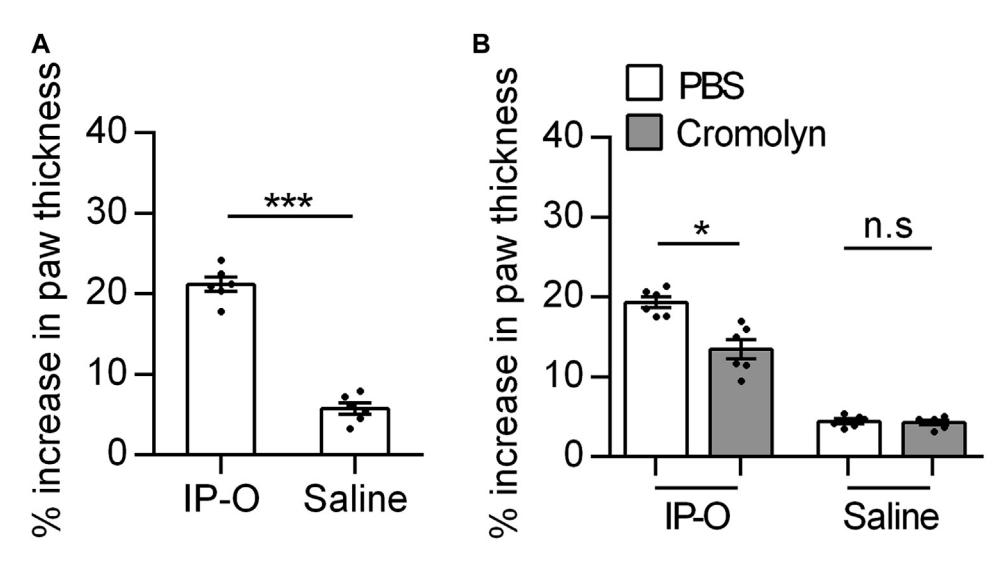


**FIG E13.** IP-O increases the paw thickness of mice. **A**, Change in the paw thickness (%) of mice after the intraplantar injection of saline (5  $\mu$ L, *left paw*) and IP-O (5  $\mu$ L, 2 mg/mL, *right paw*). n = 6. **B**, Change in the paw thickness (%) of mice after the intraplantar injection of saline (5  $\mu$ L) and IP-O (5  $\mu$ L, 2 mg/mL) in PBS-treated mice and cromolyn-treated mice. n = 6. All data are presented as mean  $\pm$  SEM. \*P<.05; \*\*\*P<.001.

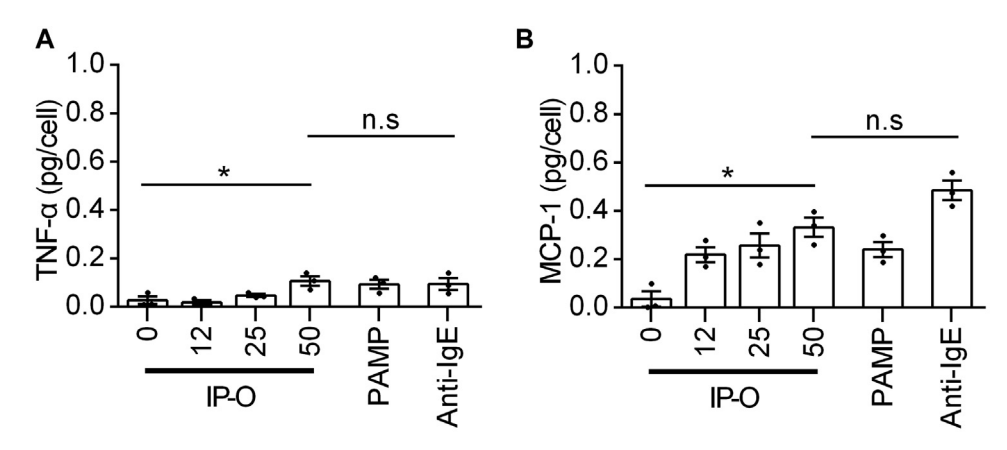


**FIG E14.** IP-O induces the release of TNF- $\alpha$  and MCP-1 from mouse PMCs. In vitro release of TNF- $\alpha$  (A) and MCP-1 (B) from mouse PMCs on stimulation by IP-O (12, 25, 50  $\mu$ mol/L), PAMP (100  $\mu$ mol/L), anti-IgE (25  $\mu$ g/mL), or vehicle alone (IP-O = 0  $\mu$ mol/L). All concentrations n = 3. All data are presented as the mean  $\pm$  SEM. \*P< .05.

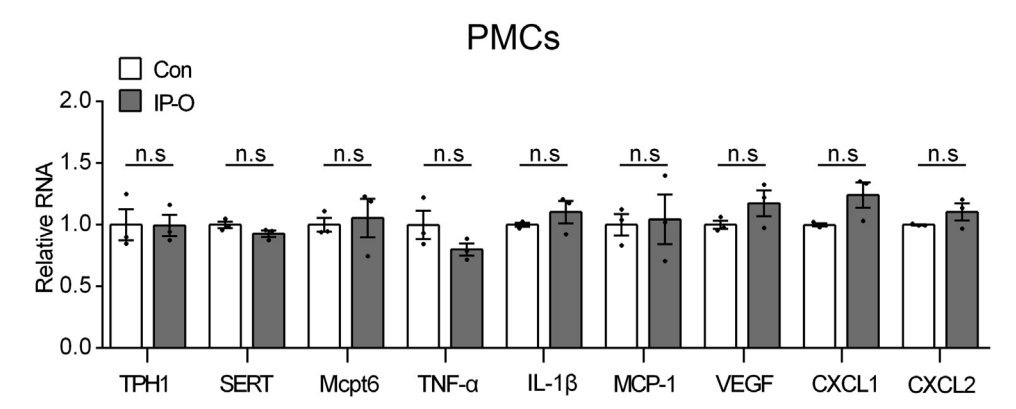


**FIG E15.** Effect of IP-O on the mRNA expression of the inflammatory cytokines and chemokines in mouse PMCs. Mouse PMCs ( $1\times10^4$  to  $5\times10^4$ ) were incubated with test substances for 30 minutes before the total intracellular RNA were collected. TPH1, serotonin transporter (*SERT*), *Mcpt6* (tryptase  $\beta$ 2), TNF- $\alpha$ , IL-1 $\beta$ , MCP-1, VEGF, CXCL1, and CXCL2 were analyzed by qPCR. All groups n=3. All data are presented as the mean  $\pm$  SEM.

TABLE E1. The qRT-PCR primer sequences for the test mouse cytokines and chemokines

Name	Direction	Sequence (5'-3')
ТРН1	+	ACGTTCCTCTCTGGCTGAA
	_	TAGCACGTTGCCAGTTTTTG
SERT	+	TCACATATGCGGAGGCAATA
	_	CTATCCAAACCCAGCGTGAT
Mcpt6	+	CATTGATAATGACGAGCCTCTCC
	_	CATCTCCCGTGTAGAGGCCAG
TNF-α	+	TAGCCAGGAGGAGAACAGA
	_	CCAGTGAGTGAAAGGGACAGA
IL-1β	+	TACATCAGCACCTCACAAGC
	_	AGAAACAGTCCAGCCCATACT
MCP-1	+	TTAAAAACCTGGATCGGAACCAA
	_	GCATTAGCTTCAGATTTACGGGT
VEGF	+	CAACTTCTGGGCTCTTCTCG
	_	CCTCTCCTCTTCCTTCCC
CXCL1	+	GTCAGTGCCTGCAGACCATG
	_	TGACTTCGGTTTGGGTGCAG
CXCL2	+	GCCAAGGGTTGACTTCAAGA
	_	TTCAGGGTCAAGGCAAACTT
GAPDH	+	AGGTCGGTGTGAACGGATTTG
	-	TGTAGACCATGTAGTTGAGGTCA